NAVAL POSTGRADUATE SCHOOL

MONTEREY, CALIFORNIA

THESIS

IMPROVED DENSITY-FUNCTIONAL TIGHT BINDING POTENTIALS FOR METALLOID ALUMINUM CLUSTERS

by

Joon H. Kim

June 2016

Thesis Advisor: Joseph Hooper

Approved for public release; distribution is unlimited

THIS PAGE INTENTIONALLY LEFT BLANK

REPORT DOCUMENTATION PAGE			*Form Approved OMB No. 0704–0188*

1. AGENCY USE ONLY *(Leave blank)*	**2. REPORT DATE** June 2016	**3. REPORT TYPE AND DATES COVERED** Master's thesis

4. TITLE AND SUBTITLE IMPROVED DENSITY-FUNCTIONAL TIGHT BINDING POTENTIALS FOR METALLOID ALUMINUM CLUSTERS	**5. FUNDING NUMBERS**
6. AUTHOR(S) Joon H. Kim	
7. PERFORMING ORGANIZATION NAME(S) AND ADDRESS(ES) Naval Postgraduate School Monterey, CA 93943-5000	**8. PERFORMING ORGANIZATION REPORT NUMBER**
9. SPONSORING /MONITORING AGENCY NAME(S) AND ADDRESS(ES) N/A	**10. SPONSORING / MONITORING AGENCY REPORT NUMBER**

11. SUPPLEMENTARY NOTES The views expressed in this thesis are those of the author and do not reflect the official policy or position of the Department of Defense or the U.S. Government. IRB Protocol number ____N/A____.

12a. DISTRIBUTION / AVAILABILITY STATEMENT Approved for public release; distribution is unlimited	**12b. DISTRIBUTION CODE**

13. ABSTRACT (maximum 200 words)

In this thesis, we study the feasibility of improving aluminum-carbon repulsive potentials for use in density-functional tight binding (DFTB) simulations of low-valence aluminum metalloid clusters. These systems are under consideration for use as novel fuels with rapid metal combustion kinetics, and contain an unusual mix of low-valence metal/metal bonds as well as organometallic components. We show that current DFTB parametrizations of the repulsive potential for Al/C interactions do not provide an adequate treatment of the bonding in these clusters. We performed a re-parametrization of the Al-C repulsive potential via comparison to high-level density functional theory (DFT) results that are known to give accurate thermochemistry for these clusters. We found that the reparametrized system solves the most egregious issues, particularly those associated with an unphysical distortion of the η^5 Al/cyclopentadienyl bond. DFTB molecular dynamics simulations of the oxidation of $Al_4Cp^*_4$ show reasonable comparison with a DFT-based Car-Parrinello method, including correct prediction of hydride transfers from Cp* to the metal centers during the reaction.

14. SUBJECT TERMS improved, density, functional, tight, binding, potentials, metalloid, aluminum clusters	**15. NUMBER OF PAGES** 73
	16. PRICE CODE

17. SECURITY CLASSIFICATION OF REPORT	**18. SECURITY CLASSIFICATION OF THIS PAGE**	**19. SECURITY CLASSIFICATION OF ABSTRACT**	**20. LIMITATION OF ABSTRACT**
Unclassified	Unclassified	Unclassified	UU

NSN 7540–01-280-5500 Standard Form 298 (Rev. 2–89) Prescribed by ANSI Std. 239–18

THIS PAGE INTENTIONALLY LEFT BLANK

Approved for public release; distribution is unlimited

IMPROVED DENSITY-FUNCTIONAL TIGHT BINDING POTENTIALS FOR METALLOID ALUMINUM CLUSTERS

Joon H. Kim
Lieutenant, United States Navy
B.S., Cornell University, 2007

Submitted in partial fulfillment of the
requirements for the degree of

MASTER OF SCIENCE IN APPLIED PHYSICS

from the

NAVAL POSTGRADUATE SCHOOL
June 2016

Approved by: Joseph Hooper, Ph.D.
Thesis Advisor

Kevin B. Smith, Ph.D.
Chair, Department of Physics

THIS PAGE INTENTIONALLY LEFT BLANK

ABSTRACT

In this thesis, we study the feasibility of improving aluminum-carbon repulsive potentials for use in density-functional tight binding (DFTB) simulations of low-valence aluminum metalloid clusters. These systems are under consideration for use as novel fuels with rapid metal combustion kinetics, and contain an unusual mix of low-valence metal/metal bonds as well as organometallic components. We show that current DFTB parametrizations of the repulsive potential for Al/C interactions do not provide an adequate treatment of the bonding in these clusters. We performed a re-parametrization of the Al-C repulsive potential via comparison to high-level density functional theory (DFT) results that are known to give accurate thermochemistry for these clusters. We found that the reparametrized system solves the most egregious issues, particularly those associated with an unphysical distortion of the η^5 Al/cyclopentadienyl bond. DFTB molecular dynamics simulations of the oxidation of $Al_4Cp^*_4$ show reasonable comparison with a DFT-based Car-Parrinello method, including correct prediction of hydride transfers from Cp* to the metal centers during the reaction.

THIS PAGE INTENTIONALLY LEFT BLANK

TABLE OF CONTENTS

I. BACKGROUND 1
- **A. ROCKET PROPELLANTS 1**
- **B. ALUMINUM CYCLOPENTADIENYL CLUSTERS 1**
- **C. DENSITY FUNCTIONAL TIGHT BINDING 2**

II. PRINCIPLES OF DENSITY FUNCTIONAL TIGHT BINDING 5
- **A. DENSITY FUNCTIONAL THEORY 5**

III. FITTING THE REPULSIVE POTENTIAL 9
- **A. CHARACTERIZING REPULSIVE POTENTIAL 9**
- **B. FITTING THE REPULSION 11**
  - **1. Collecting Data 11**
  - **2. Fitting Equations 12**
  - **3. Fitting Procedure 13**

IV. TESTING THE NEW REPULSIVE POTENTIAL 17
- **A. GEOMETRY OPTIMIZATION 17**
  - **1. Monomers 17**
  - **2. Tetramers 20**
  - **3. Systems of Greater Complexity 23**
  - **4. Bond Lengths 25**
- **B. ELECTRONIC STRUCTURE CALCULATIONS 29**
- **C. MOLECULAR ORBITALS AND ENERGY LEVELS 32**
- **D. MOLECULAR DYNAMICS 42**

V. CONCLUSIONS 47
- **A. PERFORMANCE 47**
- **B. FUTURE WORK 47**

APPENDIX A. FUNDAMENTAL CONSTANTS 49

APPENDIX B. ALUMINUM-CARBON REPARAMETRIZATION 51

LIST OF REFERENCES 53

INITIAL DISTRIBUTION LIST 55

LIST OF FIGURES

Figure 1. AlCp Monomer 10

Figure 2. Example Force-Based Fitting of the Boron-Nitrogen Repulsion Parametrization 13

Figure 3. Forces of Al-C Interaction Systems 14

Figure 4. Repulsive Potential V_{rep} from This Work and the Matsci-0-3 Set. 16

Figure 5. AlCp Monomer—Side and Head-on Views 18

Figure 6. AlCp* Monomer—Side and Head-on Views 19

Figure 7. $AlCp^{*Pr}$ Monomer—Head-on Views 20

Figure 8. AlCp Tetramer (Al_4Cp_4) 21

Figure 9. AlCp* Tetramer ($Al_4Cp^*_4$) 22

Figure 10. $AlCp^{*Pr}$ Tetramer ($Al_4Cp^{*Pr}_4$) 23

Figure 11. $Al_8Cp^*_4$ 24

Figure 12. $Al_{50}Cp^*_{12}$ 25

Figure 13. AlCp Orbitals 32

Figure 14. AlCp Energy Levels 33

Figure 15. AlCp* Orbitals 34

Figure 16. AlCp* Energy Levels 35

Figure 17. $AlCp^{*Pr}$ Orbitals 36

Figure 18. $AlCp^{*Pr}$ Energy Levels 37

Figure 19. Al_4Cp_4 Orbitals 38

Figure 20. Al_4Cp_4 Energy Levels 39

Figure 21. $Al_4Cp^*_4$ Energy Levels 40

Figure 22. $Al_4Cp^{*Pr}_4$ Energy Levels 41

Figure 23. $Al_8Cp^*_4$ Energy Levels 42

Figure 24. Al_4Cp_4 Molecular Dynamics.....44

Figure 25. $Al_3O_2Cp_3$ Molecular Dynamics 45

LIST OF TABLES

Table 1. V_{rep} Polynomial Coefficients.....15

Table 2. Bond Lengths (DFT).....26

Table 3. Bond Lengths (Reparametrized DFTB).....26

Table 4. Bond Lengths (Stock DFTB+ Matsci) – In Progress.....27

Table 5. Ring Slip Parameter η.....28

Table 6. HOMO-LUMO Gap.....29

Table 7. Binding Energy.....30

Table 8. Dipole Moment.....31

THIS PAGE INTENTIONALLY LEFT BLANK

LIST OF ACRONYMS AND ABBREVIATIONS

Cp	Cyclopentadienyl
CPU	Central Processing Unit
DFT	Density Functional Theory
DFTB	Density Functional Tight Binding
DOD	Department of Defense
SCC	Self-Consistent Charge
TB	Tight Binding

THIS PAGE INTENTIONALLY LEFT BLANK

ACKNOWLEDGMENTS

First and foremost, I would like to thank Dr. Joseph Hooper. His work ethic serves as an example for others, and his expertise in and dedication to research that supports our nation's warfighters makes him an invaluable asset to the nation.

I would also like to thank CDR Warren Tomlinson, PMP candidate, and Dr. Sufian Alnemeret, for their assistance with this research. CDR Tomlinson provided support with all DFT methods, and Dr. Alnemeret provided much expert guidance in the molecular orbitals and molecular dynamics portion of this thesis.

I would also like to thank my classmates who provided me with moral support and motivation. In addition, I would like to thank my family. I would not have this opportunity without the support they provided me to become the man I am today.

Finally, I thank God for providing me with this much-needed opportunity for rest and personal development. I truly believe this experience will make me a better officer.

THIS PAGE INTENTIONALLY LEFT BLANK

I. BACKGROUND

A. ROCKET PROPELLANTS

Solid rocket motors are widely used as missile propulsion systems in the Department of Defense (DOD) and space communities. The typical propellant grain within many of these motors consists of an aluminum fuel along with oxidizer and binder components. The aluminum particles used are typically micrometer scale, though there has been considerable recent interest in aluminum nanoparticles to increase the burning rate as well as lowering the ignition threshold [1]. Within the DOD, rockets are used in both very small systems such as the Mk 66 solid rocket motor that propels the Hydra 70 2.75 inch rocket and very large systems such as the D-5 rocket system for the Trident II missile. As such, improvements to rocket motor performance, particularly in areas of linear burn rate or energy density that may lead to novel rocket motor designs, present an attractive opportunity. Increasing the rate of aluminum combustion, however, is challenging. The process is limited by the presence of a native oxide layer on the surface of the particles, as well as the slow mass transfer that occurs during its diffusion-limited burning. Recent research efforts have been directed at developing Al nanoparticles from a different approach, using solution chemistry methods to grow small metal clusters with a single monolayer of organic ligand on their surface. These may offer the potential for greatly increased combustion kinetics, well beyond that of typical metal fuels.

B. ALUMINUM CYCLOPENTADIENYL CLUSTERS

Low-valence Al clusters with a surface organic ligand layer have been known some time, discovered in the pioneering work of Schnockel and co-workers in recent decades [2]. These clusters are formed in a co-condensation reactor which produces monovalent aluminum halide (AlCl or AlBr) liquids as the starting material. These liquids are then used for solution growth of larger clusters, which includes a ligand exchange process with, most commonly, cyclopentadienyl (C_5Me_5 or Cp^*) or hexamethyldisilazane (hmds). During the growth process, an unknown kinetic mechanism traps the system and prevents a runaway reaction which would form zero-

valent bulk metal. The final result is an onion structure with low-valent metal in the interior and organic ligands on the outside. These systems are often called "metalloid," since they contain a mix of metal-metal bonds as well as metal/organic interactions. One of the most notable cluster in this family is composed of a 50 aluminum atoms with 12 Cp^* ligands strongly bound to the exterior [2]. However, further refinement and study of these clusters is required to determine the optimal balance of reactivity, stability, and combustion properties in order to obtain a configuration suitable for safe and effective use as a rocket motor propellant or other energetic applications [1]. The most efficient approach to determine this optimal balance would be with the aid of computational studies to guide efforts of experimentalists to reproduce the desired configurations in laboratory conditions. Unfortunately, further computational study of such systems is complicated by the very large computing resource requirements for larger, more complex structures when using the current computational method of choice, density functional theory (DFT).

C. DENSITY FUNCTIONAL TIGHT BINDING

Density functional tight binding (DFTB), shows promise as an intermediate computational method that could yield approximate results practically close to the accuracy of DFT with significant reduction to computational resource requirements. Improvements in the accuracy of available density functionals, as well as the increased availability of computational resources, have made DFT the preferred computational method for electronic structure calculation for most applications [3]. It provides a good balance between the competing demands of chemical accuracy, moderate computational speed, and transferability. However, for the study of aluminum nanoparticles intended for use in rocket propellants, DFT methods prove to be quite taxing for even very large supercomputers. More in-depth analysis of systems of interest requires study of large systems, upwards of 500 atoms, evolving in time during chemical decomposition, oxidation, and similar processes. Many implementations of DFT do not scale well with the addition of more processing units (CPUs), as doubling CPUs assigned may only yield a less than 10% improvement in calculation time [4]. Therefore, the use of more approximate methods is warranted to help speed research efforts.

Though derived from DFT, DFTB is still a tight binding (TB) method with the fundamental assumption of tightly bound electrons. Therefore, it is ideally suited for covalent bound systems such as hydrocarbons [3]. Despite the known limitation of this assumption, it has also shown promising results in treating some systems with ligand protected metallic clusters (such as thiol-protected gold clusters), with the benefit of being several orders of magnitude more efficient than full Kohn-Sham DFT computation [5]. However, DFTB requires specific parametrizations to be performed to treat each type of interaction in a system, and the nature of this parametrization will greatly affect the quality and applicability of the output. As discussed below, we found that existing DFTB parametrizations in the literature are insufficient for study of the aluminum-cyclopentadienyl metalloid cluster systems. The purpose of this study is to develop a new repulsive potential parameterization that allows us to perform accurate DFTB calculations for ligated aluminum nanoparticle systems.

There are several DFTB software packages available, but the one chosen for this research was DFTB+ [6]. Several parametrization sets, in the form of Slater Koster files, are also provided by the developers free for academic use. The parameter set chosen was the matsci-0-3 parameter set, primarily selected due to its inclusion of interactions involving Al and C, which appears in every system of interest to this study [7]. The software's core development was led by Balint Aradi of the University of Bremen and Ben Hourahine of the University of Strathclyde.

THIS PAGE INTENTIONALLY LEFT BLANK

II. PRINCIPLES OF DENSITY FUNCTIONAL TIGHT BINDING

This chapter will present a brief overview of the theory of DFTB. To maintain consistency with much of the literature that provides a more in-depth study of DFTB, Hartree atomic units will be used throughout. In particular, this overview will draw heavily from [3], and all equations in this chapter are sourced exclusively from [3] to maintain consistency of terms used throughout.

A. DENSITY FUNCTIONAL THEORY

As density functional theory is the starting point for DFTB, we must have at least some understanding of the final expressions derived in DFT. For the many body problem of a system consisting of nuclei and electrons, the total energy can be written as [3]:

$$E = T + E_{ext} + E_{ee} + E_{II} \tag{1}$$

T is the kinetic energy, E_{ext} is the energy of external interactions, including electron-ion interactions, E_{ee} is the electron-electron interaction energy, and E_{II} is the ion-ion interaction energy. In Kohn-Sham DFT, with a system of non-interacting electrons, the total energy can be written as [3]:

$$E[n(r)] = T_s + E_{ext} + E_H + E_{xc} + E_{II} \tag{2}$$

T_s is the non-interacting kinetic energy, E_H is the Hartree energy, and E_{xc} is the exchange correlation (*xc*) energy. This is more explicitly written in Equation 3 below [3]:

$$E[n] = \sum_a f_a \left\langle \psi_a \left| \left(-\frac{1}{2}\nabla^2 + \int V_{ext}(\mathbf{r}) n(\mathbf{r})\right) \right| \psi_a \right\rangle + E_{xc}[n] + E_{II} \tag{3}$$

Here $f_a \in [0,2]$ is the occupation of a single-particle state ψ_a with energy ε_a. We next begin approximating by considering a system with density $n_o(\mathbf{r})$ as if atoms in the system were free and neutral. The density is not the true minimizing density that gives us our ground state energy, but we assume it is close, deviating only by some small $\delta n(\mathbf{r})$. A second order expansion of Equation 3 at $n_o(\mathbf{r})$ with fluctuation $\delta n(\mathbf{r})$ provides us with Equation 4 [3].

$$E[\delta n] = \sum_a f_a \langle \psi_a | -\frac{1}{2}\nabla^2 + V_{ext} + V_H[n_o] + V_{xc}[n_o] | \psi_a \rangle$$
$$+ \frac{1}{2}\int\int' \left(\frac{\delta^2 E_{xc}[n_o]}{\delta n \delta n'} + \frac{1}{|\mathbf{r}-\mathbf{r}'|}\right)\delta n \delta n' \qquad (4)$$
$$-\frac{1}{2}\int V_H[n_o](\mathbf{r}) n_o(\mathbf{r}) + E_{xc}[n_o] + E_{II} - \int V_{xc}[n_o](\mathbf{r}) n_o(\mathbf{r})$$

The terms in Equation 4 are normally subcategorized into energy terms. Equation 5 comes from the first line in Equation 4, and is the band structure energy [3]. Equation 6 comes from the second line, and is the energy from charge fluctuations, mainly coming from Coulomb interactions, but also containing some *xc* contributions [3]. Equation 7 is the third line, and is called the repulsive energy, because of the dominance of the ion-ion repulsion term, but also captures other *xc* effects [3].

$$E_{BS} = \sum_a f_a \langle \psi_a | H[n_o] | \psi_a \rangle \qquad (5)$$

$$E_{coul}[\delta n] = \frac{1}{2}\int\int' \left(\frac{\delta^2 E_{xc}[n_o]}{\delta n \delta n'} + \frac{1}{|\mathbf{r}-\mathbf{r}'|}\right)\delta n \delta n' \qquad (6)$$

$$E_{rep} = -\frac{1}{2}\int V_H[n_o](\mathbf{r}) n_o(\mathbf{r}) + E_{xc}[n_o] + E_{II} - \int V_{xc}[n_o](\mathbf{r}) n_o(\mathbf{r}) \qquad (7)$$

Equations 5–7 allow us to collapse Equation 4 into the more convenient form below in Equation 8 [3].

$$E[\delta n] = E_{BS}[\delta n] + E_{coul}[\delta n] + E_{rep} \qquad (8)$$

We recall that atom energy can be expressed as a function of charge fluctuation Δq, electronegativity, and the Hubbard U parameter. We make an assumption of the Coulomb energy of two spherically symmetric Gaussian charge distributions to yield Equation 9 for E_{coul} expressed as a function of charge fluctuation [3].

$$E_{coul} = \frac{1}{2}\sum_{IJ} \gamma_{IJ}(R_{IJ}) \Delta q_I \Delta q_J \qquad (9)$$

We then apply the tight binding formalism to Equation 8, which are the approximations of DFTB. In the E_{BS} term, we assume tightly bound valence electrons, and use a minimal basis set with only one radial function for each angular momentum state. The Hamiltonian matrix elements are the principal parameters for this term. In the E_{coul} term, the charge fluctuations are approximated with a Mulliken population analysis and can be parametrized by changes to the electronegativity and the Hubbard parameter U. The E_{rep} remains the repulsive energy, and is parametrized for atomic pairs.

THIS PAGE INTENTIONALLY LEFT BLANK

III. FITTING THE REPULSIVE POTENTIAL

In theory, fitting the repulsive potential V_{rep} can be performed systematically [3]. V_{rep} is considered to be analogous to E_{xc} in DFT, as it packages much of the difficult physics into a single term. However, unlike DFT, DFTB parametrization requires characterizing a new repulsion for each pair of atoms in a system, the fitting process can become very labor intensive. Additionally, individual parametrizations often require laborious adjustments that may not be fully rigorous with theory. Therefore, for this study, we chose to make use of an existing parametrization set, and limited efforts at improvement only for those parametrizations where we observed known deficiencies. More specifically, we attempted to improve only the parametrization of the Al-C interaction. The existing parametrizations that are used to treat other interactions are contained in the matsci-0-3 family of parametrizations in the DFTB+ software package [7].

A. CHARACTERIZING REPULSIVE POTENTIAL

The equations supporting parametrization of the repulsive potential are as follows and are taken from [3]:

$$V_{rep}(R) = E_{DFT}(R) - [\mathrm{E}_{BS}(R) + E_{coul}(R)] \tag{10}$$

$$N \cdot V_{rep}(R) = E_{DFT}(R) - [E_{BS}(R) + E_{coul}(R)] \tag{11}$$

Equation 10 is used for a system with a single element pair. Equation 11 is used for a symmetric structure where there are N bonds. In practice, a single system is insufficient to provide a repulsive potential that can be robustly applied to a variety of different systems with different bonding types. In the existing matsci-0-3 parametrization set, the Al-C interaction was created for the investigation of the interaction of ethylphosphonic acid ($C_2H_5PO(OH)_2$) with aluminum oxide surfaces and was fit using a CH_3-AlH_2 system [8]. As this system consists of a different bonding type from the delocalized bonding present in ligand protected metallic clusters, it would have been a reasonable assumption, even without test calculations, that a re-parametrization would be

necessary. Unsurprisingly, we observed in test calculations that re-parametrization is indeed required, as the test structure (Figure 1) shows a significant and obvious distortion in the geometry of the AlCp monomer that is a building block to our systems of interest.

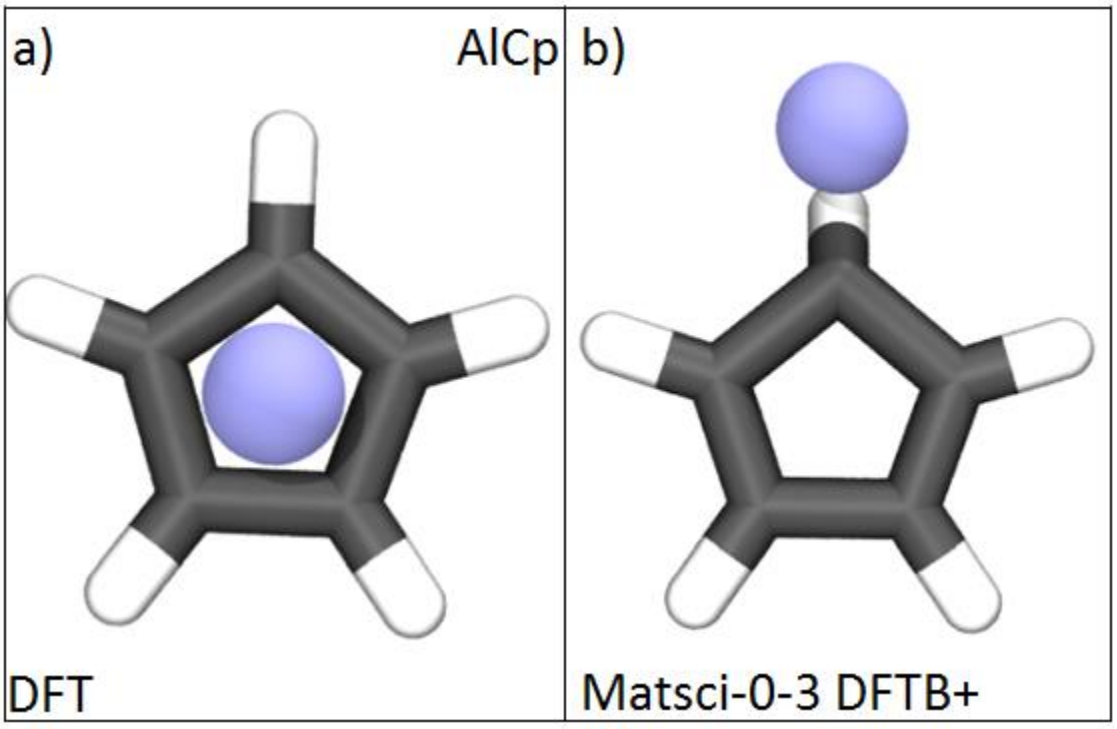

Figure 1. AlCp Monomer

Therefore, we start with relatively simple structures of interest, where DFT can still quickly provide us with geometries $\boldsymbol{R}$, energies $E_{\mathrm{DFT}}(\boldsymbol{R})$, and forces $\boldsymbol{F}^{\mathrm{DFT}}$ (which would be zero for an optimized structure). One approach would be to fit V_{rep} to minimize the energy and force differences and $|E^{\mathrm{DFT}} - E^{\mathrm{DFTB}}|$ and $|\boldsymbol{F}^{\mathrm{DFT}} - \boldsymbol{F}^{\mathrm{DFTB}}|$. However, as advised by [3], in practice, we only minimize the force difference. The reason for this recommendation is that it provides us the benefit of working with absolute terms as, unlike energies, forces are absolute terms. Additional justification is provided in that most of the energy contribution in DFTB comes from the band structure term. This term is adjusted by modifying the confinement potential and the Hubbard parameter. If we find that we need to make adjustments to minimize the energy difference at large distances, we cannot fix the errors in energy by adjusting the short-range repulsion energy alone.

Additionally, repulsion energy needs to be monotonic and smooth. If we adjust repulsion too abruptly, the parametrization's forces will suffer from the erratic repulsion. For the purposes of this study, we did not make any adjustments to the confinement potential or Hubbard parameter. Therefore, the fit is only to the forces, or the derivative of the repulsive potential, yielding [3]:

$$V'_{rep} = \frac{E_{DFT}'(R_{AB}) - [E_{BS}'(R_{AB}) + E_{coul}'(R_{AB})]}{N} \tag{12}$$

B. FITTING THE REPULSION

The systems chosen as the base of our parametrization effort were the simple CH_3-AlH_2 system used in the original matsci-0-3 parametrization, a trimethylaluminum ($Al(CH_3)_3$) system, and an aluminum cyclopentadienyl (AlCp) monomer. We can rapidly generate V'_{rep} curves for these systems by using DFT and DFTB to obtain $E_{DFT,}$ $E_{BS,}$ and E_{coul} by varying the distance R_{AB} to obtain a range of energy values as a function of $R_{AB.}$

1. Collecting Data

DFT calculations to obtain E_{DFT} for these relatively simple systems were performed by optimizing the geometries using the M06-2X functional and 6–31G* basis set in the Gaussian 09 software package. This combination of functional and basis set had been previously determined by our research group to give accurate bonding energies of aluminum metalloid clusters (typically within 5 kJ/mol of experiment).

The energy calculations to obtain E_{BS} and E_{coul} were performed using DFTB+ on the same geometries with varying R_{AB} as those used in the DFT calculations. All DFTB+ calculations were performed using Version 1.2 of the DFTB+ software package, using Parser Version 4. Repulsive interaction was characterized using the polynomial option. The Hamiltonian was calculated using SCC (self-consistent charge) calculations, with an SCC tolerance of 1.0E-6 e, and the maximum force component was 0.02 eV/ Å. Derivatives E_{DFT}', E_{BS}', and E_{coul}' were obtained with numerical differentiation.

2. Fitting Equations

The DFTB+ software package allows for a polynomial characterization of the repulsive potential as shown in Equation 13 [9]:

$$V_{rep} = \sum_{i=2}^{9} c_i (r_{cut} - r)^i \tag{13}$$

From this form of V_{rep}, we can easily obtain an expression for the derivative of the repulsive potential, with which we can then fit our data.

$$V'_{rep} = -\sum_{i=2}^{9} i c_i (r_{cut} - r)^{i-1} \tag{14}$$

$$F = -\frac{dU}{dr} \tag{15}$$

$$F = \sum_{i=2}^{9} i c_i (r_{cut} - r)^{i-1} \tag{16}$$

As the force is the negative of the derivative of potential energy, the coefficients as determined from a fit to the force can then be directly used in the polynomial equation for the repulsive potential. An example of a fitted force curve from previous literature on the boron-nitrogen interaction is provided in Figure 2 [10].

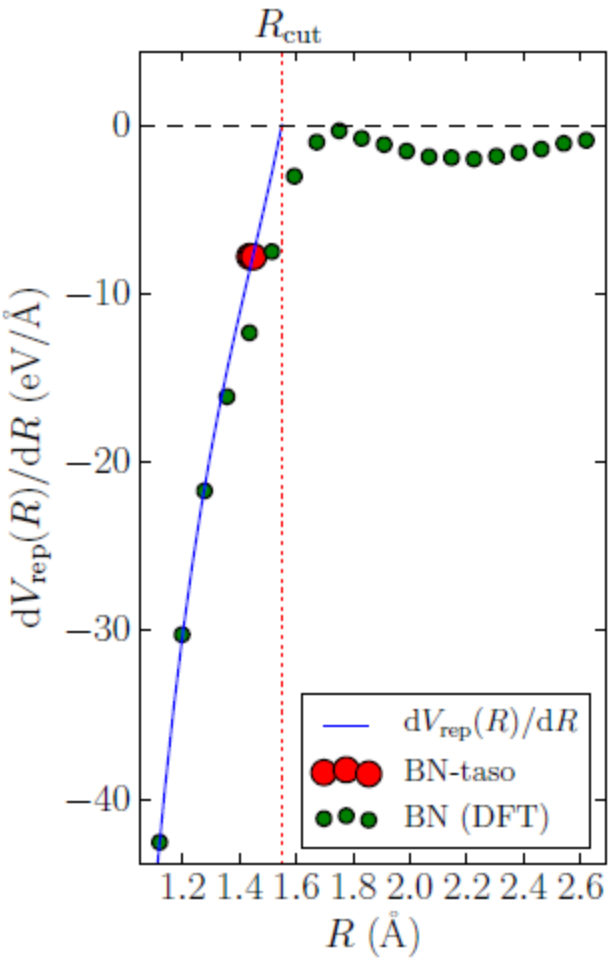

Figure 2. Example Force-Based Fitting of the Boron-Nitrogen Repulsion Parametrization

It will be clear to the most casual observation that this fitting is not in particularly good agreement with the plotted points. We will delve into the reasons for this in our discussion of the fitting procedure.

3. Fitting Procedure

An initial test fitting was made solely to AlCp using a least squares fitting algorithm to the form of the polynomial in Equation 16. For the value of r_{cut}, the original parametrization's value of 6.81 Bohr was left unchanged. Unfortunately, initial attempts using just the output of the algorithm were not wholly adequate. While fitting alone was

able to provide a result that corrected the ring slip deficiency caused by the stock matsci-0-3 parametrization in the AlCp monomer, it provided V_{rep} curves that were not well aligned with physical conventions. Therefore, small manual adjustment of the polynomial coefficients was conducted with performance testing on a family of AlCp based systems with a focus on improving the geometry results. Some compromise was required between the accuracy of the calculation and smoothness and monotonicity of the function in order to avoid compromising transferability. Specifically, in addition to the monomer, adjustments were tested against both simple covalent bonding systems and tetramer geometries. The tetramers proved to be most sensitive to adjustments to small changes to the V_{rep} of the system, with even small changes leading to distortions in the Al-Al bonding of those clusters. During this adjustment, it was observed that changes in the region of interest (between 4–5 Bohr) provided the most significant impact to the accuracy of output geometries for this family of systems.

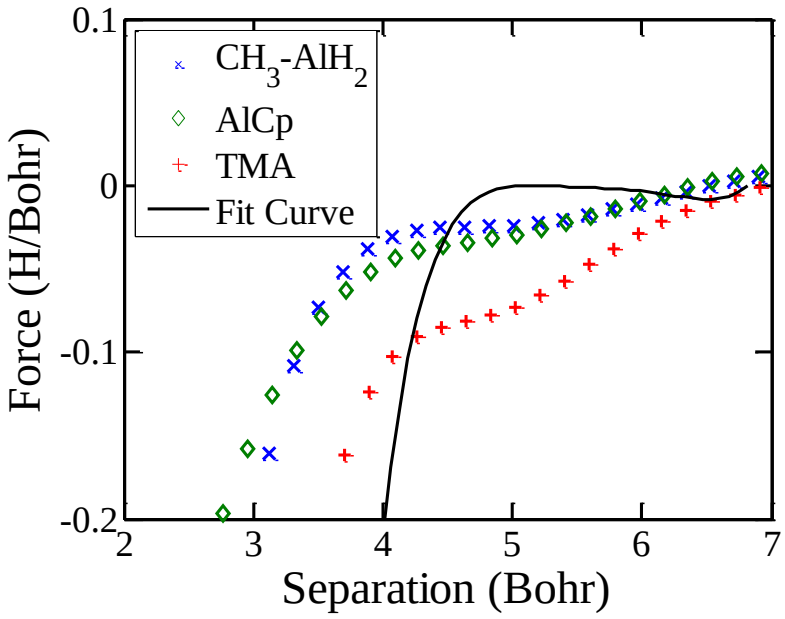

Figure 3. Forces of Al-C Interaction Systems

Figure 3 shows the fit curve for the force, which is plotted along with force curves obtained for the three systems discussed in Section 1, for which we obtained DFT data.

Visually, the force curves are not in particularly good agreement with any of the systems. The fitting algorithm alone did not produce satisfactory results when all test geometries were run, therefore manual adjustments were necessary. Manual adjustments were performed on V_{rep}, not on the force curves, therefore the fit to the force suffered. However, as seen previously in Figure 2, this kind of result is not particularly unusual in DFTB potentials. In the parametrization in Figure 2, the author chose to make adjustments to a V_{rep} curve from a strict fit to the data in order to match the results of band structure calculations for his systems.

For our parametrization, transferability to our systems of interest was the paramount concern. A spline is often used in the fitting of other DFTB parametrizations, which would provide the benefit of being able to more finely adjust fitting for experimentation with parametrization performance to isolate changes to more specific ranges of separations. However, we chose the polynomial fit due to its easier implementation of re-parametrization efforts in DFTB+. Table 1 contains the final parametrization's coefficients:

Table 1. V_{rep} Polynomial Coefficients

Coefficient	Value
c2	0.0352
c3	-0.067
c4	0.0585
c5	-0.0273
c6	0.0069
c7	-0.0010
c8	0.0001

As the coefficients obtained by fitting the force are identical to the coefficients in our repulsive potential, we can then plug these coefficients in directly to Equation 13, which provides us with our repulsive potential shown in Figure 4.

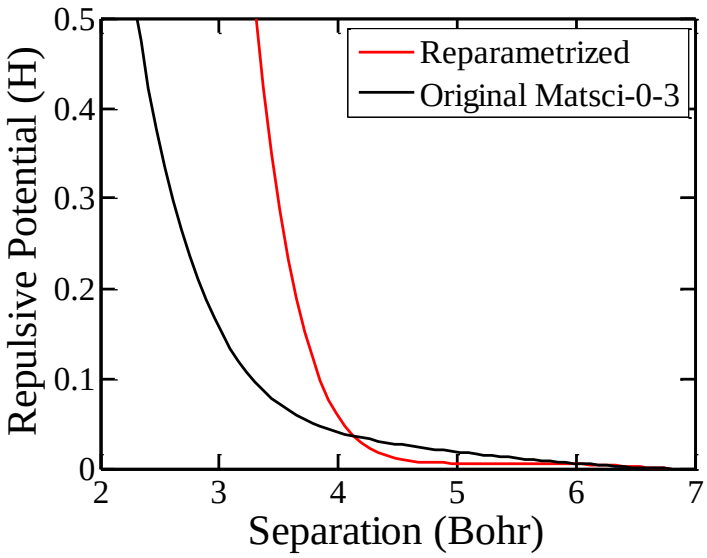

Figure 4. Repulsive Potential V_{rep} from This Work and the Matsci-0-3 Set.

Notable features in Figure 4 are that the new repulsive potential is significantly more repulsive for distances that are shorter than those typically encountered in the systems we are interested in, which is approximately where the two curves intersect, and roughly coincides with the Al-C separation found in most DFT equilibrium geometry calculations for the AlCp monomer. As we increase to distances greater than that equilibrium separation, the repulsive potential becomes significantly lower.

IV. TESTING THE NEW REPULSIVE POTENTIAL

We begin testing our new repulsive potential with an examination of the output geometries. DFT calculations for these systems were run using the Gaussian 09 software package, using the 6–31G* basis set and M06-2X functional. The only exception was the $Al_{50}Cp^*_{12}$ cluster, which was optimized using the B3LYP functional. DFTB calculations were run with DFTB+ Version 1.2, using both the stock matsci-0-3 parameter set and a modified matsci-0-3 parameter set using the reparametrized Al-C interaction.

A. GEOMETRY OPTIMIZATION

In addition to a qualitative examination of the geometries obtained through DFTB, we also performed measurements of the bond lengths to perform a quantitative examination of our new repulsive potential's performance. We also measure the η parameter, which quantifies how well the bonding of the Al atom is centered on the Cp ring. The η parameter is also considered to be represent how many of the ring C atoms are bonded to the central Al atom [11]. An η^5 value would correspond to equal bonding between the Al atom and each of the five C ring atoms, while an η^1 value would correspond to bonding predominantly between the Al atom and just one of the five C ring atoms.

1. Monomers

The first system is the same that was used to demonstrate the deficiencies in the current Al-C parametrization in the DFTB+ matsci-0-3 parameter set. The AlCp monomer is the most basic building block for the ligand protected aluminum clusters we are interested in. Figure 4 shows the geometries, with Figures 5a and 5d depicting the structure optimized with DFT, Figure 5b and 5e depicting the structure optimized with the original DFTB parameter set, and Figure 5c and 5f depicting the structure optimized with the reparametrized DFTB parameter set.

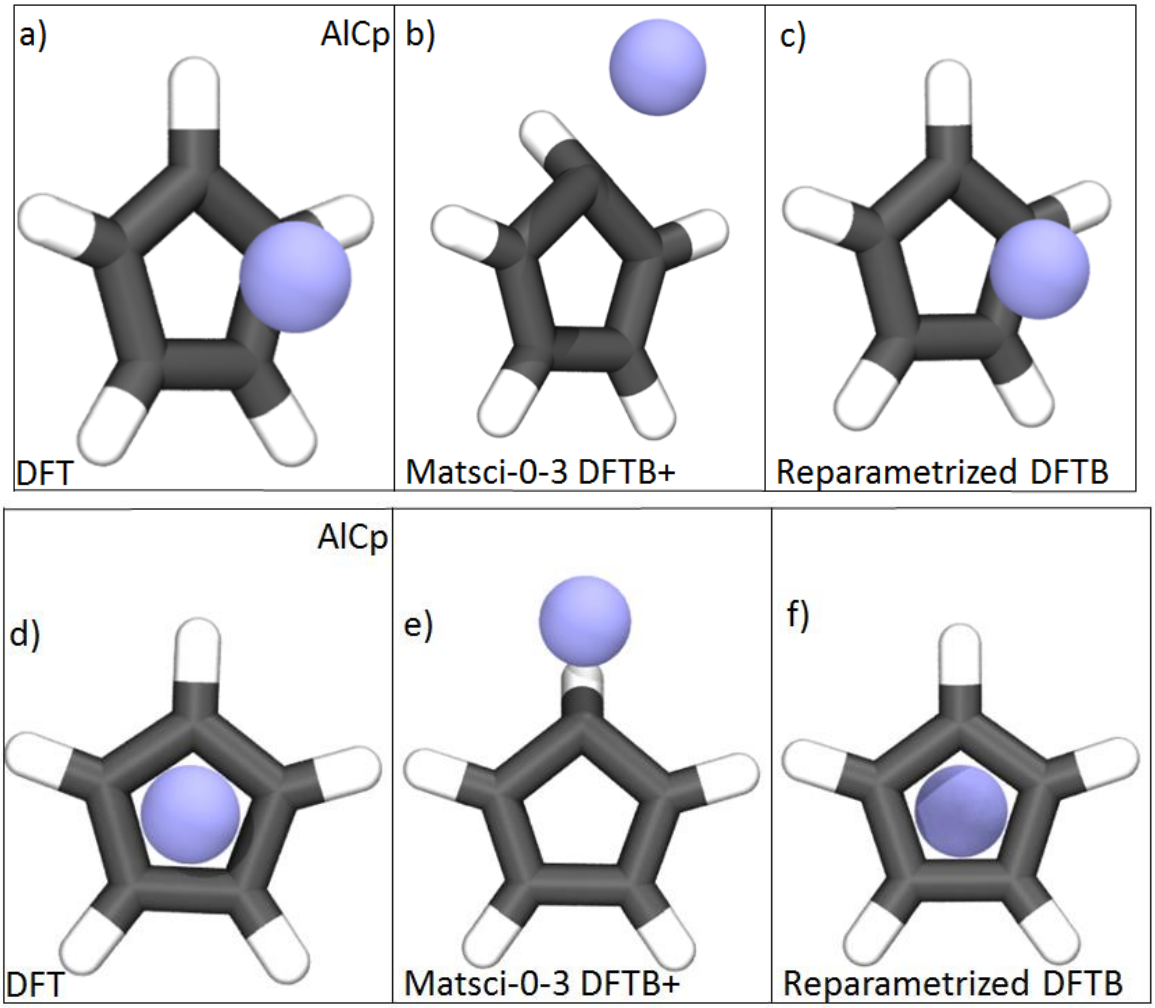

Boxes a) and d) depict DFT optimization. Boxes b) and e) depict stock DFTB+ optimization. Boxes c) and f) depict reparametrized DFTB+ optimization. Note the shifting of the Al atom and distortion in the Cp ring present in stock DFTB+ optimization that is corrected in the reparametrized DFTB optimization.

Figure 5. AlCp Monomer—Side and Head-on Views

A qualitative visual inspection of the geometries reveals that the optimized geometry produced by a reparametrized DFTB calculation provides a reasonably close approximation to the DFT geometry. The visually apparent distortion due to ring slip in the bonding between the Al atom and the Carbon ring in the AlCp molecule is no longer present, as the Al atom is properly centered in the η^5 position.

Figure 6 depicts an AlCp* monomer, which is a methylated AlCp, with a CH_3 methyl group replacing each H atom attached to each C atom on the AlCp carbon ring. It

is of greater interest as a component of more complex ligand protected aluminum clusters that hold promise in energetics applications. Figure 6a and 6d present the DFT optimized structure, Figures 6b and 6e present the results of the original DFTB parameter set, and Figures 6c and 6f are from the reparametrized DFTB parameter set.

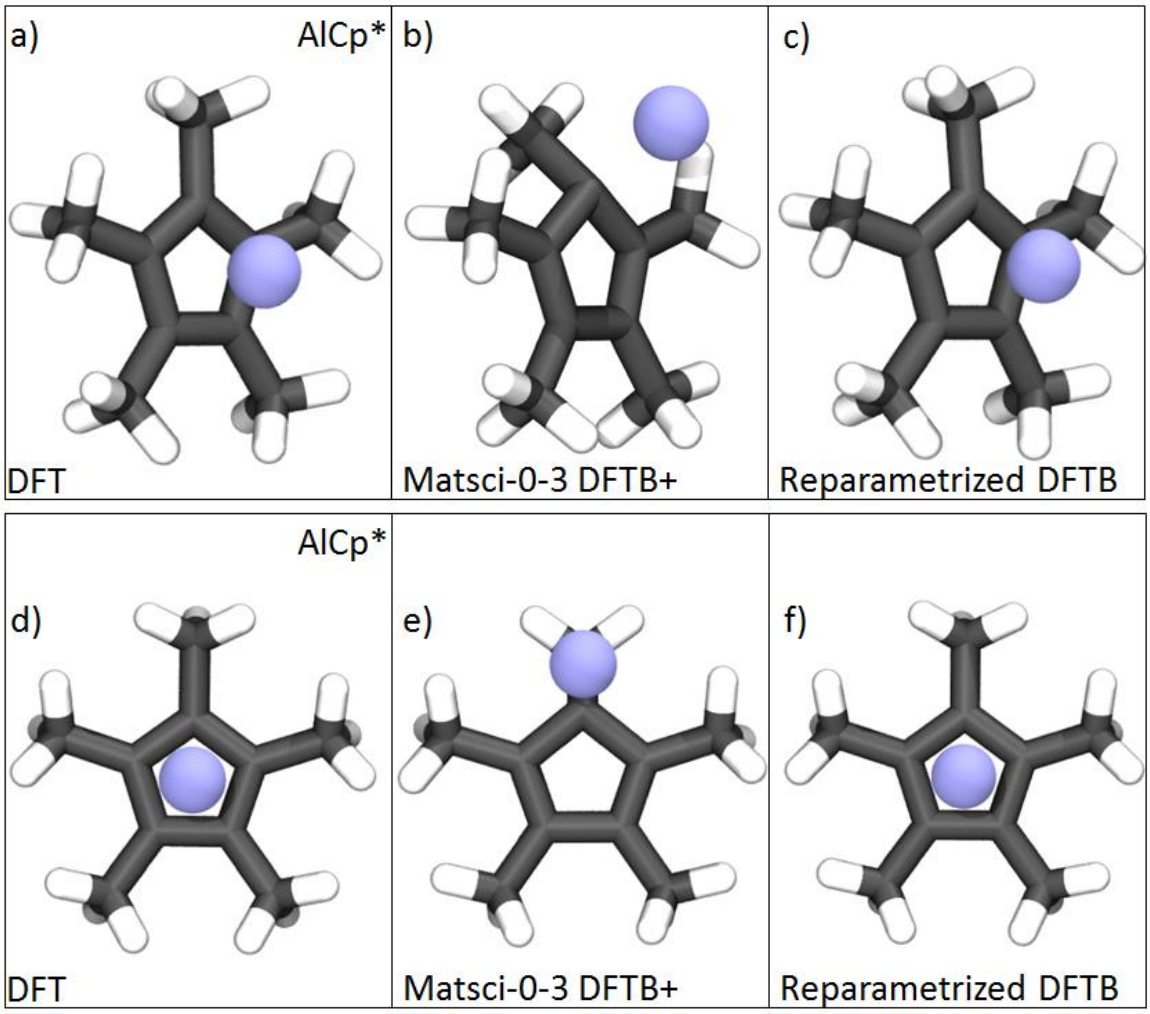

Boxes a) and d) depict DFT optimization. Boxes b) and e) depict stock DFTB+ optimization. Boxes c) and f) depict reparametrized DFTB+ optimization. Reparametrized interaction is again necessary to correct the Al atom shift and Cp ring distortion.

Figure 6. AlCp* Monomer—Side and Head-on Views

The reparametrized DFTB result is again reasonably close visually to the DFT result, and offers a significant improvement over the original DFTB parametrization,

which, similar to the AlCp results, shifts the Al atom significantly from the correct η^5 position.

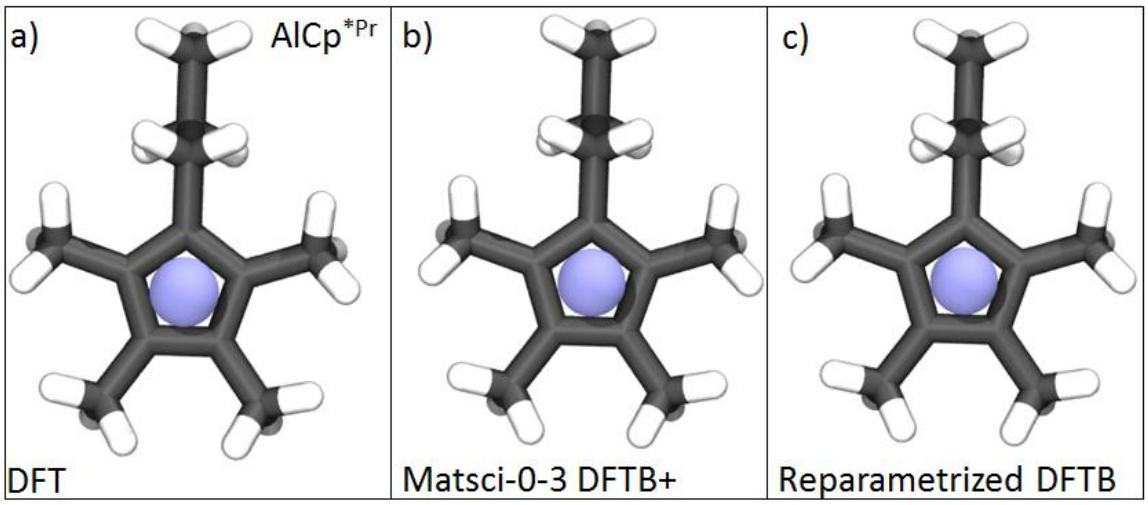

Box a) depicts DFT optimization. Box b) depicts stock DFTB+ optimization. Box c) depicts reparametrized DFTB+ optimization. Surprisingly, the stock DFTB+ parameter set does not cause clearly apparent distortion for this particular monomer.

Figure 7. $AlCp^{*Pr}$ Monomer—Head-on Views

Figure 7 depicts an $AlCp^{*Pr}$ monomer, which removes one of the methyl groups from the AlCp* monomer, and replaces it with a propyl group. In these views, the propyl group is attached to the top of the ring. Once again, the reparametrized DFTB provides a visually satisfying approximation of the DFT result. What is surprising is the original DFTB result also does not present any obvious distortion to the geometry from the DFT result. However, as stated previously when discussing the fitting strategy, visually satisfactory results in monomer optimization did not necessarily carry over to the next level in complexity for these structures, as will be discussed further in the next section.

2. Tetramers

Figure 8 shows an AlCp tetramer (Al_4Cp_4), formed by combining four AlCp monomers with the core Al atoms in a tetrahedral shape. The deficiency in the original DFTB parametrization is very apparent in this view, as the core Al atoms maintain the proper configuration, the Cp rings both tilt and shift from their correct positions, and

there is also noticeable distortion in the Cp ring, as the H atom closest to the Al atom bonded to the ring begins to tilt its bond out and away the ring configuration.

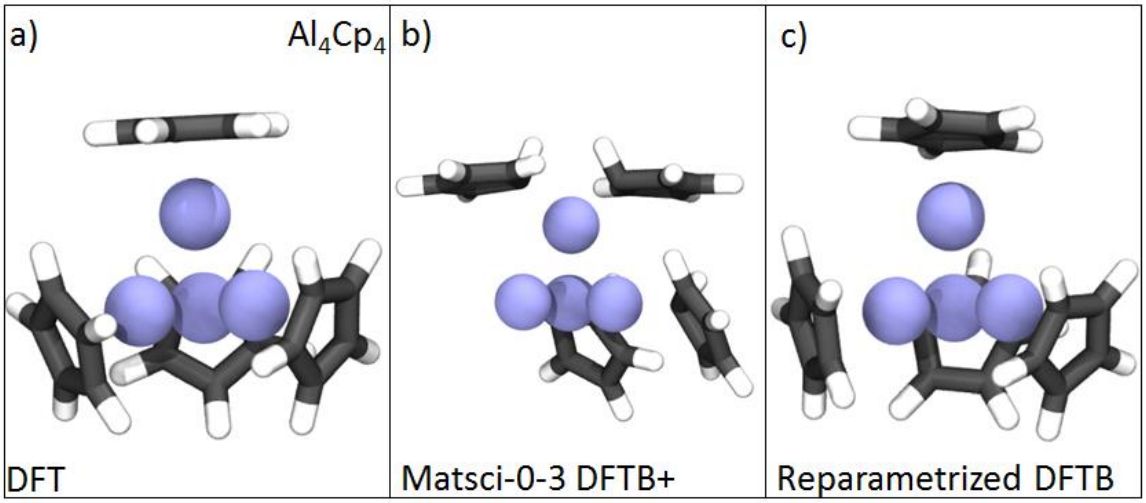

Box a) depicts DFT optimization. Box b) depicts stock DFTB+ optimization. Box c) depicts reparametrized DFTB+ optimization. This tetramer exhibits a carryover of the distortion present in its component monomers. The reparametrized DFTB result closely approximates the DFT result.

Figure 8. AlCp Tetramer (Al_4Cp_4)

Similar issues are apparent in Figure 9, which depicts an AlCp* tetramer ($Al_4Cp^*_4$). Here the Cp ring also tilts and shifts, with the same distortion in the Cp ring, except in this case, the methyl group, which has replaced the H closest to the Al atom, tilts away from the ring. The reparametrized DFTB result significantly improves upon these deficiencies, and appears to be in good agreement with DFT results.

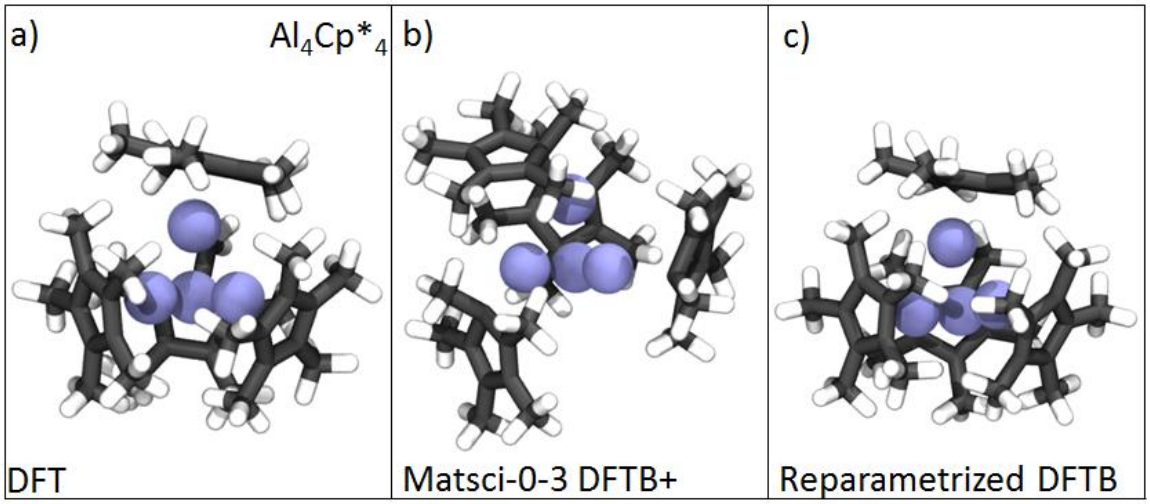

Box a) depicts DFT optimization. Box b) depicts stock DFTB+ optimization. Box c) depicts reparametrized DFTB+ optimization. As in the previous image, the tetramer carries over the distortion of its component monomers, which is corrected by the reparametrized DFTB interaction.

Figure 9. AlCp* Tetramer ($Al_4Cp^*_4$)

The final tetramer $Al_4Cp^{*Pr}_4$ reveals similar issues as the other tetramer systems. Significant shift is evident in the ligand positioning from the proper positions around the Al core in the stock DFTB+ optimization depicted in Figure 10b. This occurs despite the visually satisfying monomer in Figure 7b. Distortion of the ligand itself is present as well, with the Propyl groups being tilted out and away. This further validates a need to extend some testing to more complicated systems before final selection of a parametrization of the repulsive potential. Once again, the reparametrized potential corrects the visually evident deficiencies.

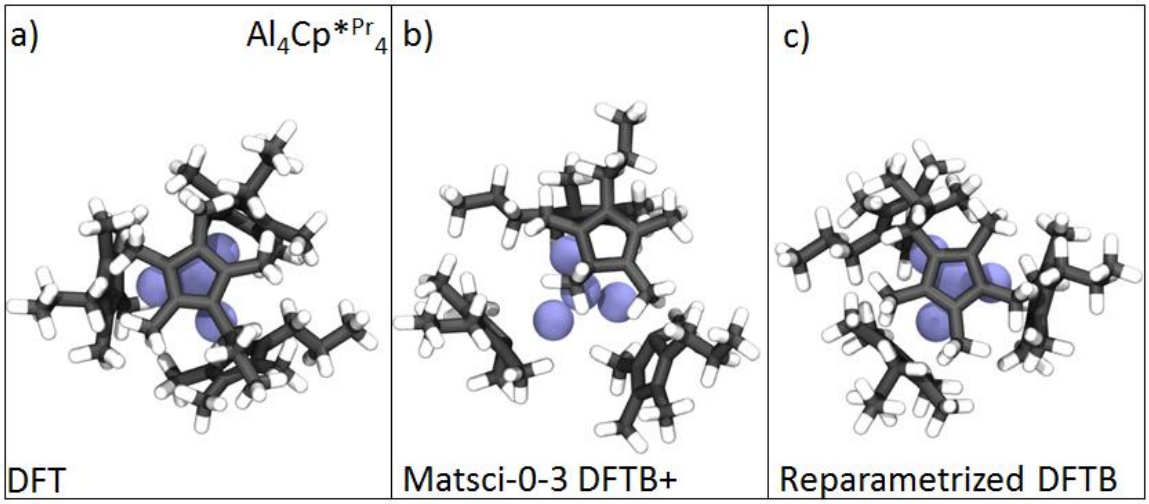

Box a) depicts DFT optimization. Box b) depicts stock DFTB+ optimization. Box c) depicts reparametrized DFTB+ optimization. Despite the visually satisfactory result in the component monomer, the stock parametrization leads to the same category of distortion in the other tetramers in this family of systems.

Figure 10. $AlCp^{*Pr}$ Tetramer ($Al_4Cp^{*Pr}_4$)

3. Systems of Greater Complexity

Unfortunately, DFTB is still approximate relative to DFT, and with a very limited scope of change, we encounter some trouble with more complex systems. The first system with an added layer of complexity, $Al_8Cp^*_4$, is depicted in Figure 11, and is closely related to the tetramer $Al_4Cp^*_4$. It adds 4 Al atoms to the Al core in the tetramer $Al_4Cp^*_4$.

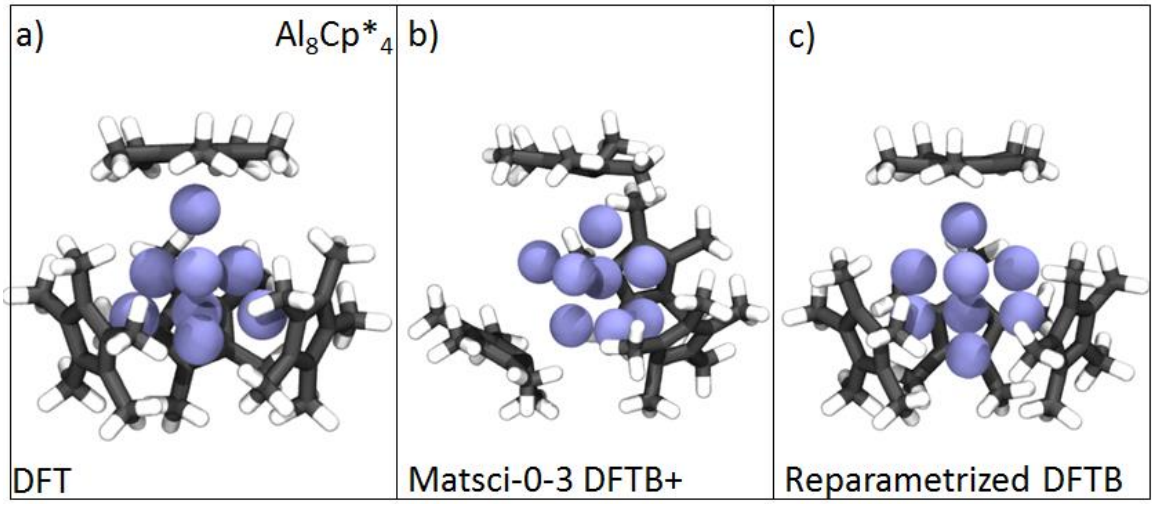

Box a) depicts DFT optimization. Box b) depicts stock DFTB+ optimization. Box c) depicts reparametrized DFTB+ optimization. The stock DFTB+ parametrization exhibits significant asymmetric shifting of the Al core in addition to the shifting and distortion of the Cp* ligands. However, the reparametrized DFTB result causes some distortion in the Al-Al core as well.

Figure 11. $Al_8Cp^*_4$

Unsurprisingly, the stock DFTB parametrization causes similar distortion in both the Cp* ligand positioning about the core, as well as within the ligands themselves. And again, the reparametrized DFTB result correctly positions the Cp* ligands about the core, without any apparent distortion in the ligands. However, we do see some differences in the Al_8 core. In the DFT optimized structure, we see that the Al_8 core is a single tetrahedron of 4 aluminum atoms, with an inverted tetrahedron that is contained inside the larger outer tetrahedron. In our new DFTB result, the inner tetrahedron expands outside the boundary formed by the outer tetrahedron.

A system of great interest and of far greater complexity is $Al_{50}Cp^*_{12,}$ depicted in Figure 12. This system is the type of cluster with potential for use in rocket fuels and other energetics, as it contains a sizable internal aluminum nanocluster with protective ligands.

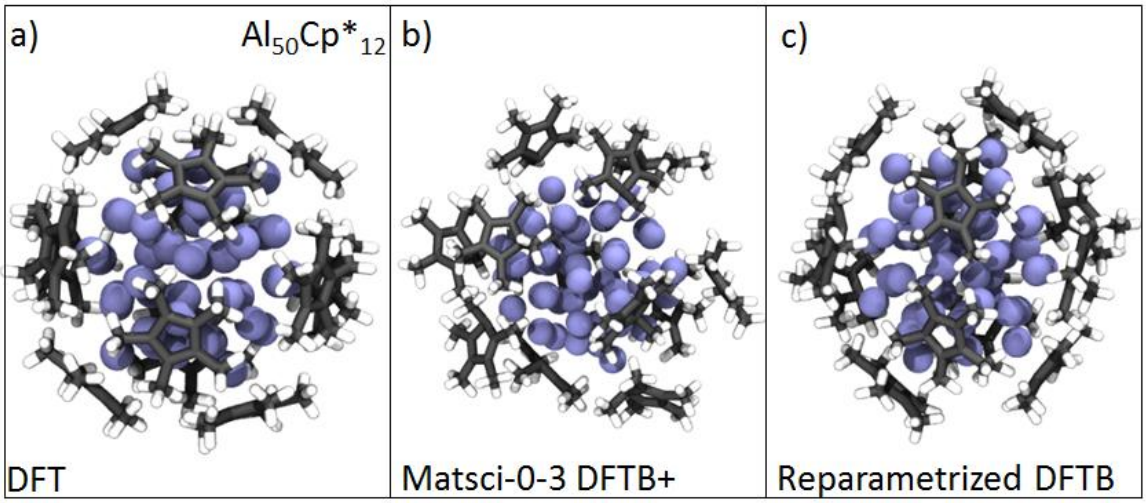

Box a) depicts DFT optimization. Box b) depicts stock DFTB+ optimization. Box c) depicts reparametrized DFTB+ optimization. The stock DFTB+ parametrization exhibits significant asymmetric shifting within the Al core in addition to shifting and distortion of the Cp* ligands. There is no obvious distortion in the Al core with the reparametrized DFTB result, however, some Cp* ligands shift from their DFT positions.

Figure 12. $Al_{50}Cp^*_{12}$

The resulting calculations again demonstrate some of the limitations of the approximate method. While it does improve visibly upon the results of the stock DFTB parametrization, it is not able to match the DFT result completely. Specifically, the Cp* rings in the new parametrization begin to demonstrate a slight tilt, though the positioning of the ligands themselves is not significantly inferior. Additionally, the new parametrization improves upon the significant distortion to the internal Al core present in the stock parametrization.

4. Bond Lengths

A comparison of bond lengths provides us with a more quantitative means of evaluating the accuracy of DFTB relative to DFT. The bond lengths of interest are the C-C distances (in the Carbon ring in the Cp component), the Al-C distances (for more complex structures, between the Cp ring and its bonded Al atom), the Al-Al distances (where applicable) and the C-H distances. We are also interested in the Ring Slip distance, which is defined to be the distance between the perpendicular projection of the bonded Al atom onto the plane of its corresponding C_5 ring and the center of the C_5 ring.

This distance is used to determine the η parameter, or hapticity, which has been categorized by [10] as: η^5 (0 Å), η^3 (0.8 Å), η^2 (1.0 Å), and η^1 (>1.2 Å).

Table 2. Bond Lengths (DFT)

Cluster	Al-C (Å)	Al-Al (Å)	C-C Ring Carbons (Å)	C-H(Å)
AlH_2CH_3	1.953	-	-	1.094
Tri-Methyl-Aluminum	1.960	-	-	1.094
AlCp	2.35	-	1.413	1.079
AlCp*	2.32	-	1.424	1.095
$AlCp^{*Pr}$	2.325	-	1.424	1.095
Al_4Cp_4	2.357	2.721	1.416	1.082
$Al_4Cp^*_4$	2.331	2.768	1.423	1.096
$Al_4Cp^{*Pr}_4$	2.335	2.783	1.423	1.096
$Al_8Cp^*_4$	2.250	2.629	1.427	1.095

Table 3. Bond Lengths (Reparametrized DFTB)

Cluster	Al-C (Å)	Al-Al (Å)	C-C Ring Carbons (Å)	C-H(Å)
AlH_2CH_3	2.261	-	-	1.105
Tri-Methyl-Aluminum	2.264	-	-	1.106

AlCp	2.46	-	1.425	1.097
AlCp*	2.48	-	1.434	1.112
AlCp*^{Pr}	2.48	-	1.434	1.112
Al_4Cp_4	2.49	2.807	1.425	1.097
$Al_4Cp^*_4$	2.51	2.806	1.433	1.115
$Al_4Cp^{*Pr}_4$	2.51	2.806	1.433	1.115
$Al_8Cp^*_4$	2.5	2.768	1.433	1.113

Table 4. Bond Lengths (Stock DFTB+ Matsci) – In Progress

Cluster	Al-C (Å)	Al-Al (Å)	C-C Ring Carbons (Å)	C-H(Å)
AlH_2CH_3	1.970	-	-	1.110
Tri-Methyl-Aluminum	1.980	-	-	1.108
AlCp	3.354	-	1.437	1.104
AlCp*	3.087	-	1.216	1.112
AlCp*^{Pr}	2.705	-	1.432	1.113
Al_4Cp_4	3.351	2.769	1.033	1.103
$Al_4Cp^*_4$	3.058	2.775	1.215	1.115
$Al_4Cp^{*Pr}_4$	3.049	2.769	1.219	1.114
$Al_8Cp^*_4$	3.3072	2.775	1.446	1.112

Table 5. Ring Slip Parameter η

Cluster	DFT, η parameter, (Å)	Reparametrized DFTB, η parameter, (Å)	Stock matsci-0-3 DFTB, η parameter, (Å)
AlCp	0.00017 (η^5)	0.0001 (η^5)	2.825 (η^1)
AlCp*	0.00022 (η^5)	0.0011 (η^5)	0.963 (η^2)
AlCp*^{Pr}	0.00703 (η^5)	0.0013 (η^5)	0.0252 (η^5)
Al_4Cp_4	0.00307 (η^5)	0.0166 (η^5)	2.405 (η^1)
$Al_4Cp^*_4$	0.04801 (η^5)	0.0335 (η^5)	2.678 (η^1)
$Al_4Cp^{*Pr}_4$	0.06371 (η^5)	0.025 (η^5)	1.032 (η^2)
$Al_8Cp^*_4$	0.38842 (η^5)	0.0031 (η^5)	-

All reparametrized DFTB and DFT results have η^5 values of hapticity.

The ring slip for the stock DFTB matsci parametrization produces unacceptably large shifts in η value.

The quantitative data in Tables 2–5 supports the qualitative assessment of the geometry visualizations. The stock matsci-0-3 parametrization demonstrates significant problems throughout the family of aluminum cyclopentadienyl clusters. More specifically, we see that the Al-C bond lengths are significantly longer (almost 1 Å in the worst case) than our DFT results. We can also quantify the ring slip and η parameter, with all but one monomer shifting to the η^1 or η^2 position. However, it does performs well for simpler C-Al bonds, such as those found in the CH_3-AlH_2 (used in the original matsci-0-3 parametrization) and trimethylaluminum ($Al(CH_3)_3$) systems.

The Al-C, Al-Al, C-C, and C-H distances of both the reparametrized DFTB results and the DFT results show good agreement. C-C and C-H bond lengths for clusters computed with reparametrized DFTB and DFT are less than 0.01 Å apart, Al-Al

distances are well within 0.1 Å, and C-Al distances are within 0.2 Å. However, we lose some transferability to more conventional Al-C bonds, with CH_3-AlH_2 and trimethylaluminum ($Al(CH_3)_3$) bond lengths becoming approximately 0.3 Å longer than DFT or the stock DFTB results. However, this is an acceptable penalty for study of the systems we are interested in, as these types of Al-C bonds are not expected in the reacted products.

B. ELECTRONIC STRUCTURE CALCULATIONS

The HOMO-LUMO gap is the energy difference between the highest occupied molecular orbital (HOMO) and lowest unoccupied molecular orbital (LUMO). We can see in Table 6 that the DFTB result consistently underestimates the HOMO-LUMO gap in comparison to the DFT result. Interestingly, the amount by which DFTB underestimates the HOMO-LUMO gap is consistent within each family of systems. For the monomers, the underestimation is approximately 0.8 eV, while the tetramers underestimate by approximately 2.0 eV. The $Al_8Cp^*_4$, which is somewhat structurally similar to the tetramers has a difference of approximately 2.6 eV.

Table 6. HOMO-LUMO Gap

Cluster	DFT (eV)	DFTB (eV)
AlCp	5.869	5.090
AlCp*	5.624	4.874
$AlCp^{*Pr}$	5.616	4.866
Al_4Cp_4	4.832	2.831
$Al_4Cp^*_4$	4.626	2.623
$Al_4Cp^{*Pr}_4$	4.586	2.663
$Al_8Cp^*_4$	3.643	1.031

This result is not unreasonable, as the Slater-Koster files for the matsci parameter set for these elements indicate that it was originally built using the LDA functional. The HOMO-LUMO gap for our DFT calculations were performed with the M062X

functional, and comparison testing indicated that LDA functionals also underestimated the HOMO-LUMO gap in comparison for these systems relative to the M062X functional. Recall from Equation 12 that DFT energy is key to building the DFTB parametrization. Therefore, we expect that this underestimation of the HOMO-LUMO gap is inherited from the LDA functional the matsci parameter set was originally built on. However, LDA performs well for treatment of ligand interaction with bulk materials [12]. Therefore, it was believed that continuing to base our parametrizations on the LDA functional would provide better transferability to larger clusters.

Table 7. Binding Energy

Cluster	DFT (kJ/mol)	DFTB (kJ/mol)	Measured (kJ/mol)
Al_4Cp_4	140	98.8	-
$Al_4Cp^*_4$	159	142	150
$Al_4Cp^{*Pr}_4$	167	143	160

The binding energy of the tetramers is calculated by taking the difference between the total energy of the tetramer and the total energy of four of the component monomers, and is presented in Table 7. The DFTB result shows that the tetramers are slightly weakly bound in comparison to DFT. The DFT M062X functional was specifically chosen to give good agreement between DFT calculated binding energy values and two known experimental values [13]. For the two experimentally validated systems, we have generally good agreement between DFT and DFTB. Additionally, the magnitude of difference between our reparametrized DFTB results and DFT results are significantly better than that which was seen with some other DFT functionals.

Table 8. Dipole Moment

Cluster	DFT (Debye)				DFTB (Debye)			
	x	y	z	total	X	y	z	total
AlCp	1.126	-0.0006	-0.0007	1.13	0.747	-0.00061	-0.00104	0.747
AlCp*	-0.001	0.0008	-1.780	1.78	-0.0618	0.120	-0.381	0.404
AlCp*^{Pr}	-0.470	-0.0001	-1.791	1.85	0.0952	-0.00000062	0.364	0.376
Al_4Cp_4	-0.0051	0.0075	-0.0154	0.0179	-0.110	0.0389	0.0602	0.131
$Al_4Cp^*_4$	0.0519	0.0705	-0.134	0.160	-0.307	-0.0237	-0.131	0.334
$Al_4Cp^{*Pr}_4$	-0.0289	-0.0104	-0.0798	0.0855	0.0199	0.0311	0.0141	0.0396
$Al_8Cp^*_4$	0.0389	-0.0068	0.0255	0.0470	0.00628	0.00497	-0.00312	0.0086

Dipole moment calculations from our DFTB results present some significant discrepancies in the monomers. As we see in Table 8, for the monomers, DFT is in good agreement with qualitative expectations, aligning the dipole moment to have a strong component along whichever axis is passing through the center of the Cp ring. Though this is still somewhat present in the DFTB results, both the total magnitude and directionality of the dipole moment is not in good agreement with the DFT results. This becomes particularly problematic for the AlCp* and AlCp*^{Pr} monomers. This is somewhat consistent with plots of calculated charge density for these monomers, where we observed asymmetric charge densities around the Cp ring, clustering a concentrating a higher charge density for one of the C atoms in the Cp ring, which is not the expected result.

However, the performance improves for the tetramers (including $Al_8Cp^*_4$), where we would expect, as is predicted by DFT, that the total dipole moment would be rather

small, as the systems generally exhibit a symmetrical configuration about each core. Here there is better agreement between the DFTB and DFT results, with less than order of magnitude difference between the total dipole moment values.

C. MOLECULAR ORBITALS AND ENERGY LEVELS

The DFTB+ software package includes a molecular orbital plotting utility called waveplot. We used this utility to plot the molecular orbitals for monomers and investigated its applicability for tetramers as well.

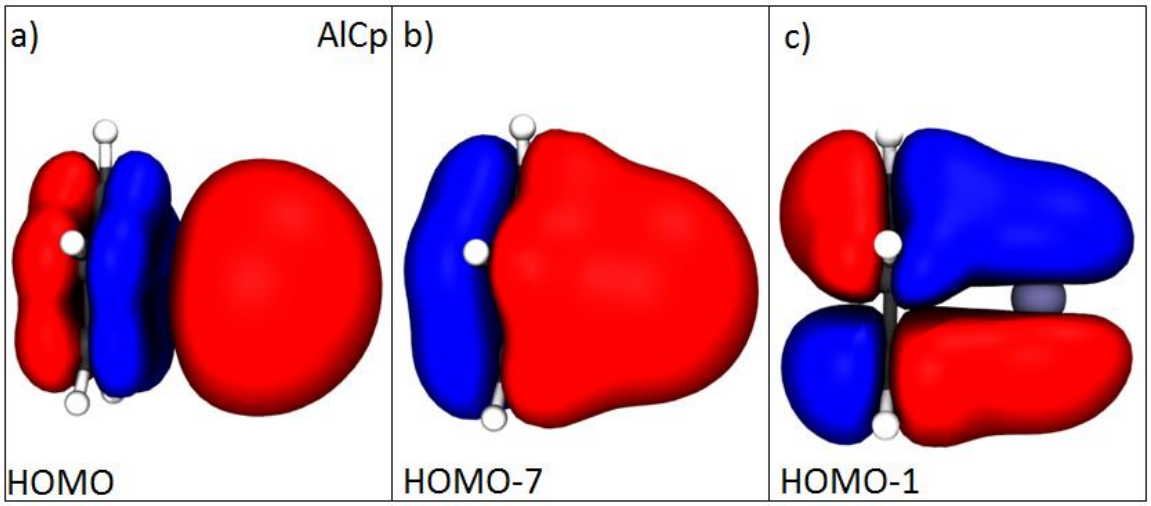

Box a) depicts the HOMO for AlCp and its nonbonding interaction between the Cp a_1 and the Al *sp*, Box b) depicts the HOMO-7 for AlCp and its Cp a_1 bonding interaction with the Al *sp*, and Box c) depicts the HOMO-1 for AlCp and overlap between the Al p and the Cp e_1.

Figure 13. AlCp Orbitals

For the simplest system, AlCp, we see results that provide good agreement between the DFTB molecular orbitals and the corresponding calculated molecular orbitals as calculated from DFT in previous research. The DFT calculations for the molecular orbitals were performed with the B3LYP DFT functional using the 6–31(g,p) basis set [12]. The molecular orbitals depicted here are three of the bonding orbitals for AlCp, the HOMO, HOMO-1, and HOMO-7 (Figure 13) and correspond to those calculated in [12].

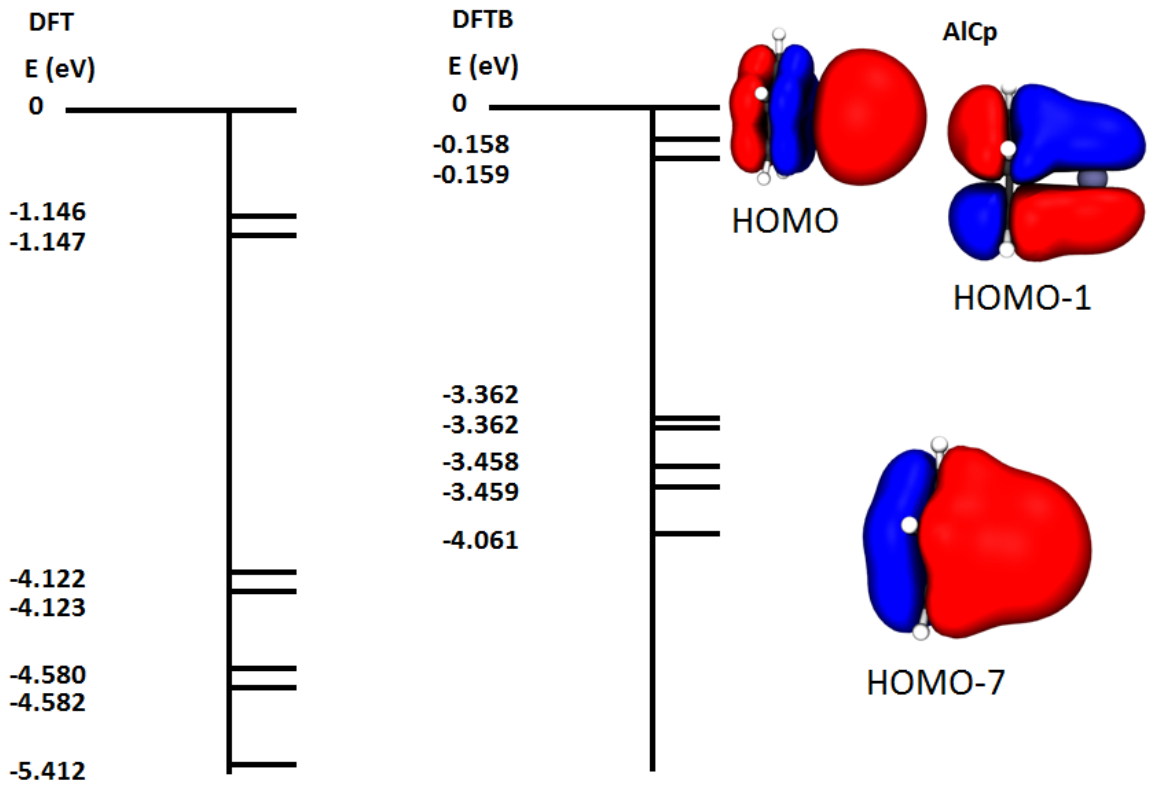

Figure 14. AlCp Energy Levels

With the energy levels, we observe in Figure 14 that DFTB underestimates the energy levels of the orbitals relative to our DFT results. The degenerate pairing of molecular orbital energies is consistent between both DFTB and DFT. The corresponding orbital energies are shifted down by approximately between 1.0 eV to 1.3 eV from DFT to DFTB.

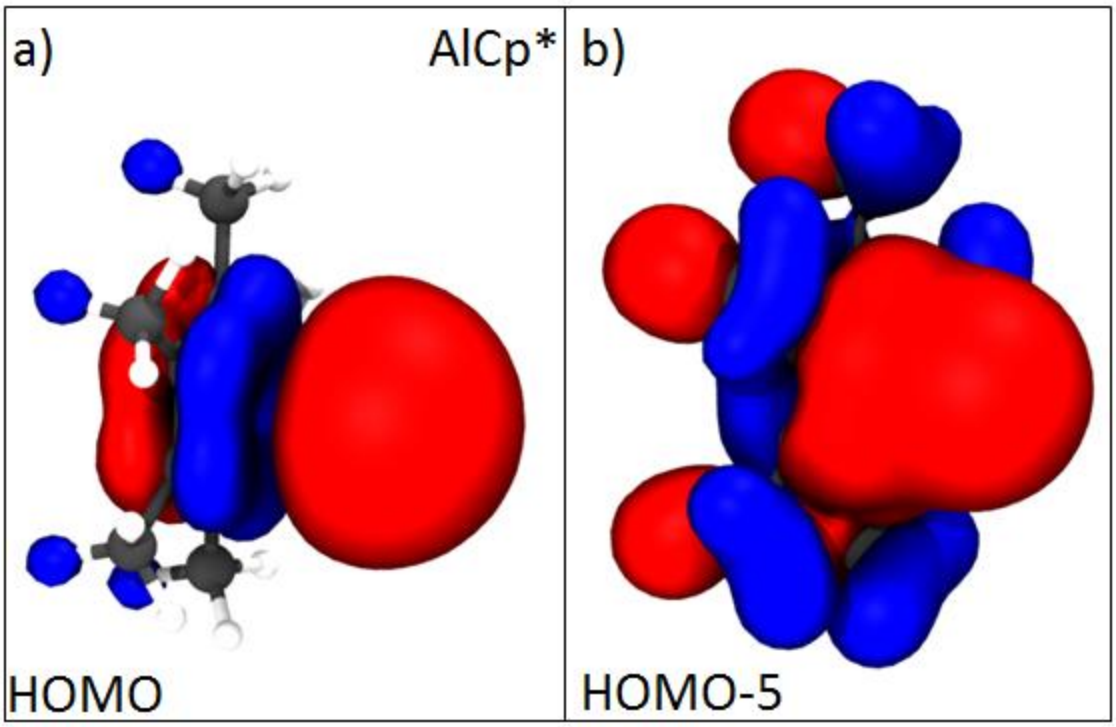

Box a) depicts the HOMO for AlCp* and its nonbonding interaction between the Cp a_1 and the Al *sp* as well as an additional contribution from the added methyl groups, Box b) depicts the HOMO-5 for AlCp* and its Cp a_1 bonding interaction with the Al *sp* as well as the additional contribution from the added methyl groups.

Figure 15. AlCp* Orbitals

For the AlCp* system (Figure 15), we can see good parallels with the AlCp system's molecular orbitals. Here the HOMO is generally in good agreement with the HOMO for the AlCp system, though with notable differences accounting for the addition of the methyl groups to the outside of the Cp ring. The HOMO-5 is analogous to the HOMO-7 for AlCp, again with additional orbital contribution corresponding to the added methyl groups. However, no analogous molecular orbital for the HOMO-1 in AlCp could be found for AlCp*.

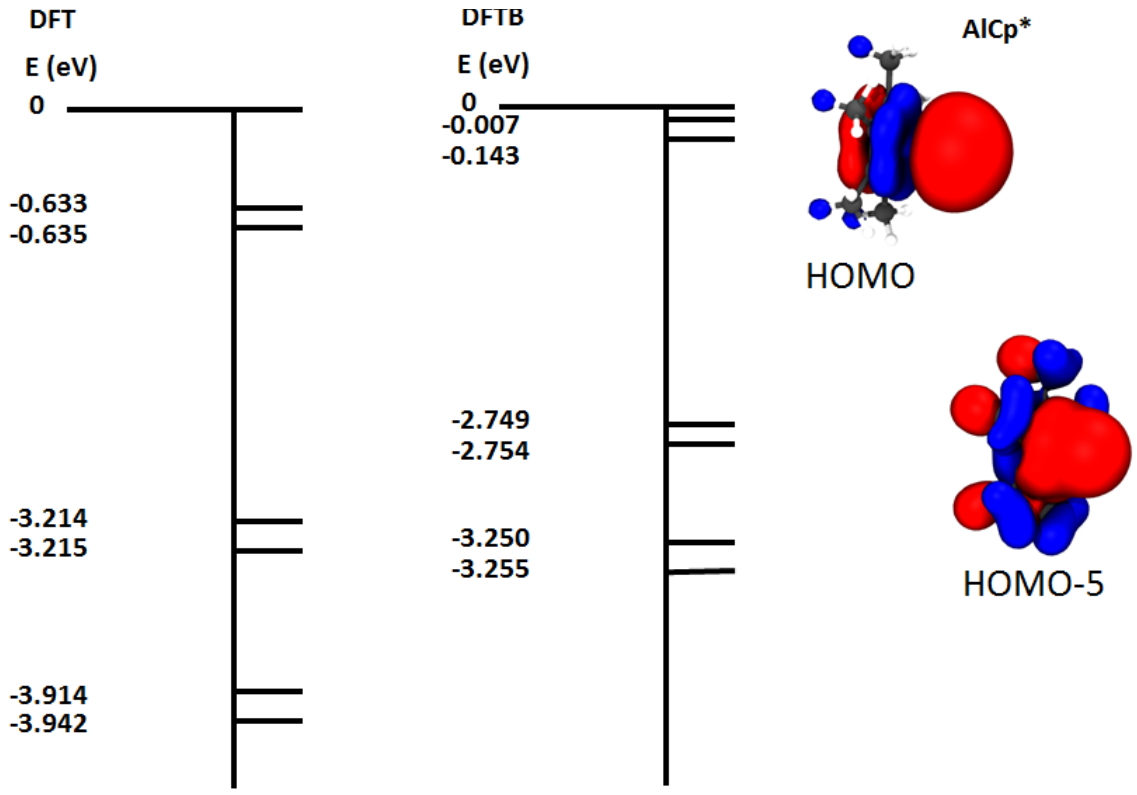

Figure 16. AlCp* Energy Levels

Once again, our results (Figure 16) indicate that DFTB underestimates the energy levels of the orbitals relative to our DFT results while the degenerate pairing remains consistent. The corresponding orbital energies are shifted down by approximately between 0.5 eV to 0.7 eV from DFT to DFTB.

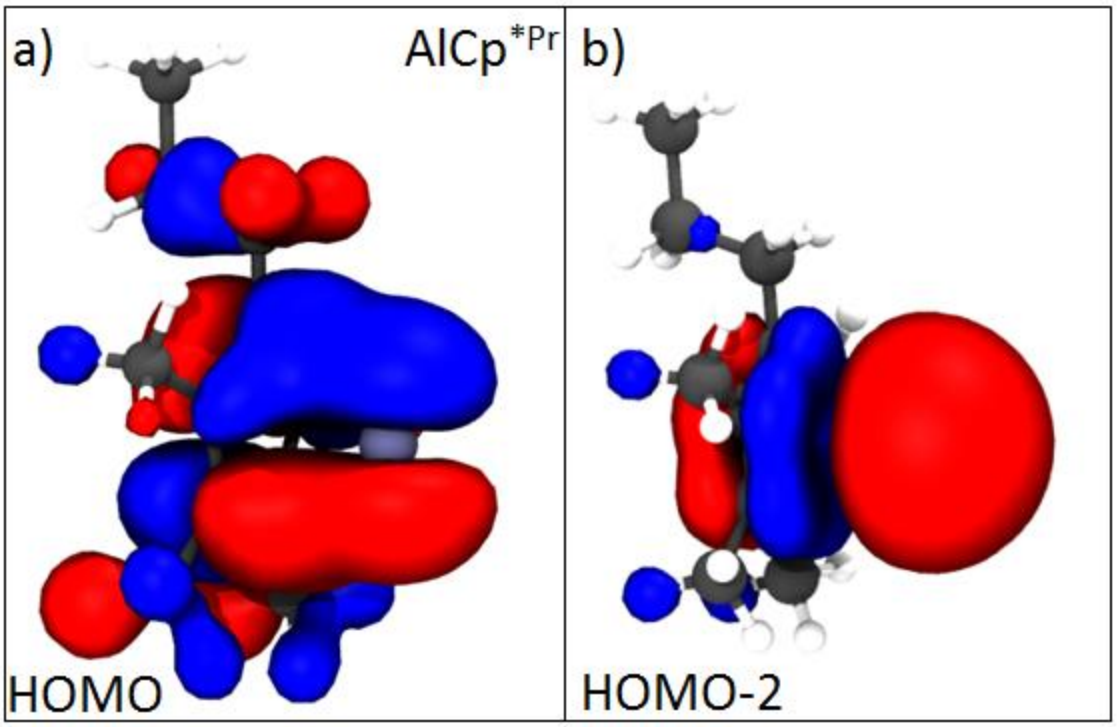

Box a) depicts the HOMO for AlCp*^{Pr} and overlap between the Al p and the Cp e_1 as well as an additional contribution from the attached Propyl group, Box b) depicts the HOMO-2 for AlCp*^{Pr} its nonbonding interaction between the Cp a_1 and the Al *sp* as well as the additional contribution from the attached Propyl group. Note that the relative ordering of the HOMO and HOMO-2 for this system is in reverse order from the analogous systems in AlCp.

Figure 17. AlCp*^{Pr} Orbitals

For the AlCp*^{Pr} system (Figure 17), we again see orbitals analogous to those found in AlCp. However, there is no system analogous to the HOMO-7 of AlCp. Additionally, the HOMO of AlCp*^{Pr} is analogous to the HOMO-1 of AlCp, and the HOMO-2 of AlCp*^{Pr} is analogous to the HOMO of AlCp, indicating that the relative ordering of those bonding orbitals is switched. A possible explanation for this behavior appears in Figure 18.

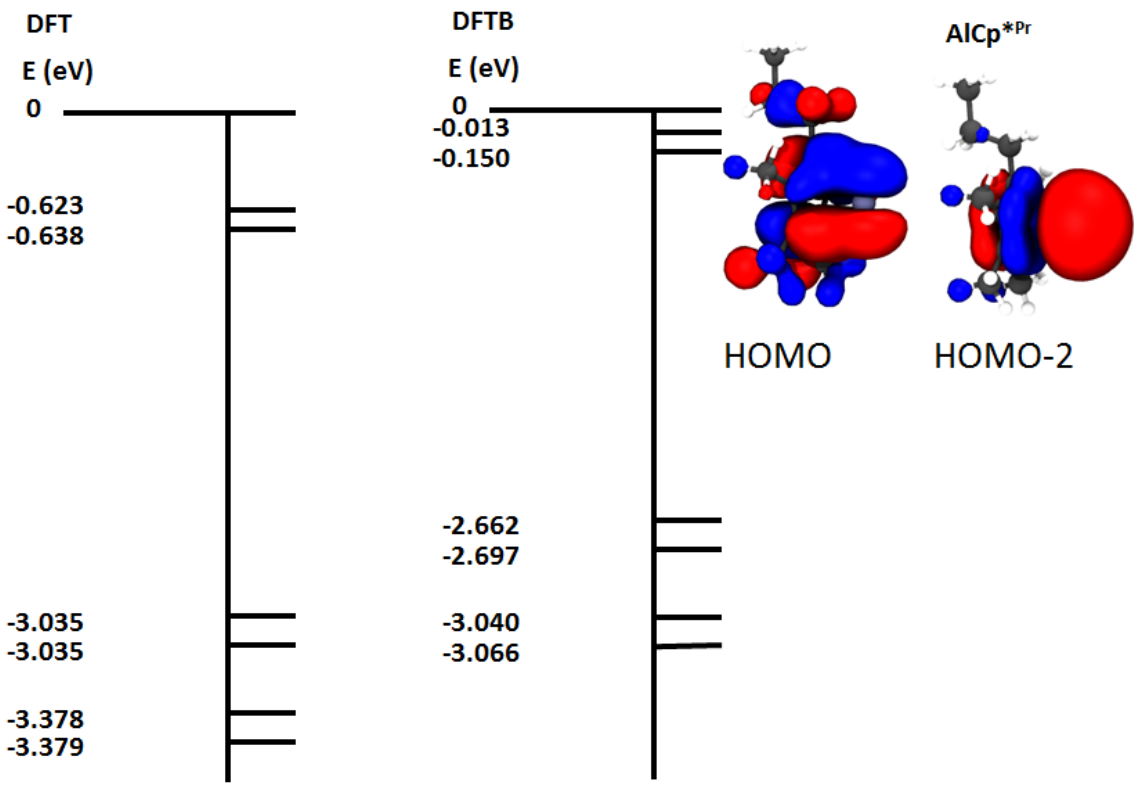

Figure 18. AlCp*^{Pr} Energy Levels

Figure 18 shows a possible explanation for the change in ordering of the HOMO and HOMO-2 orbitals of AlCp*^{Pr} relative to AlCp's analogous orbitals. The energy levels of the three highest occupied orbitals in our DFTB calculation are very close, nearly triply degenerate. The general trend for underestimating the energy levels and degenerate pairing continues for our third monomer. The corresponding orbital energies are shifted down by approximately between 0.3 eV to 0.6 eV from DFT to DFTB.

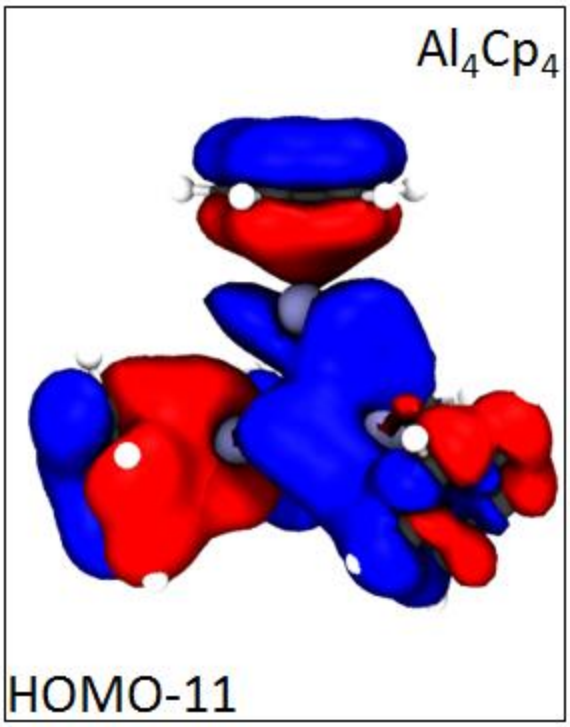

Figure 19. Al_4Cp_4 Orbitals

The applicability of waveplot calculated molecular orbitals rapidly breaks down for more complex systems. For the simplest tetramer, Al_4Cp_4, we can see in Figure 19 that the HOMO-11 orbital here does not match the equivalent bonding orbital obtained through DFT. Most notably, there is considerable asymmetry between the lower 3 ligands, as well as significant distortion around the Al core. We believe that the minimal basis set used in DFTB, while providing us with dramatic improvements in calculation speed, leads to a significant loss of accuracy for more complex systems, at least without a more thorough re-parametrization.

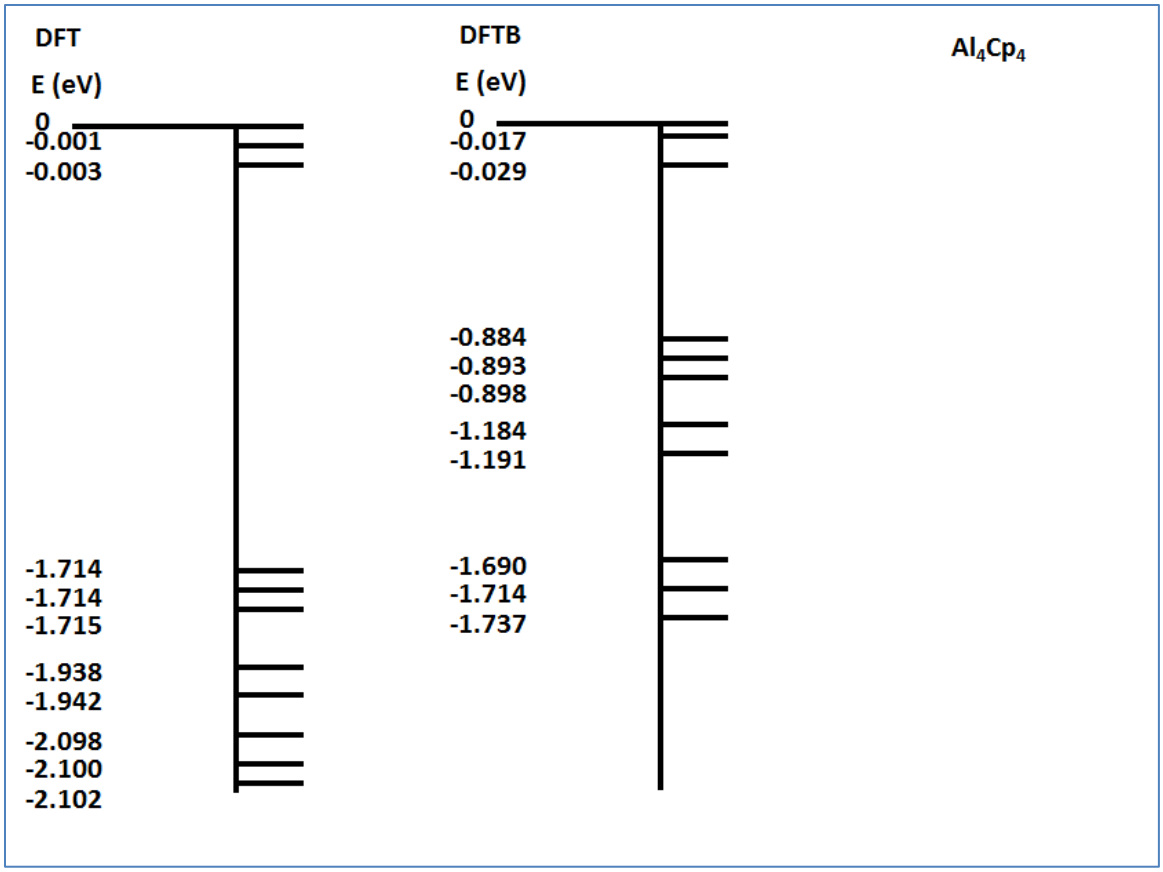

Figure 20. Al_4Cp_4 Energy Levels

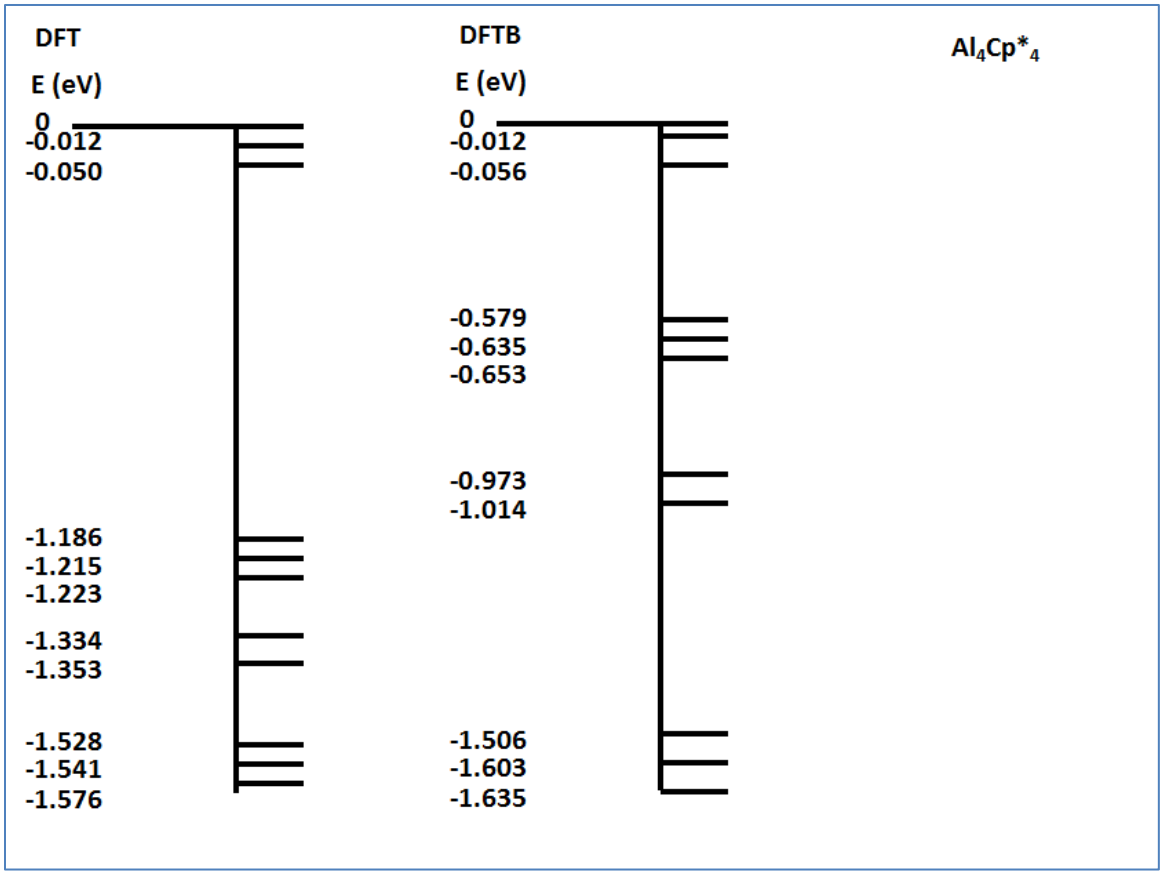

Figure 21. $Al_4Cp^*_4$ Energy Levels

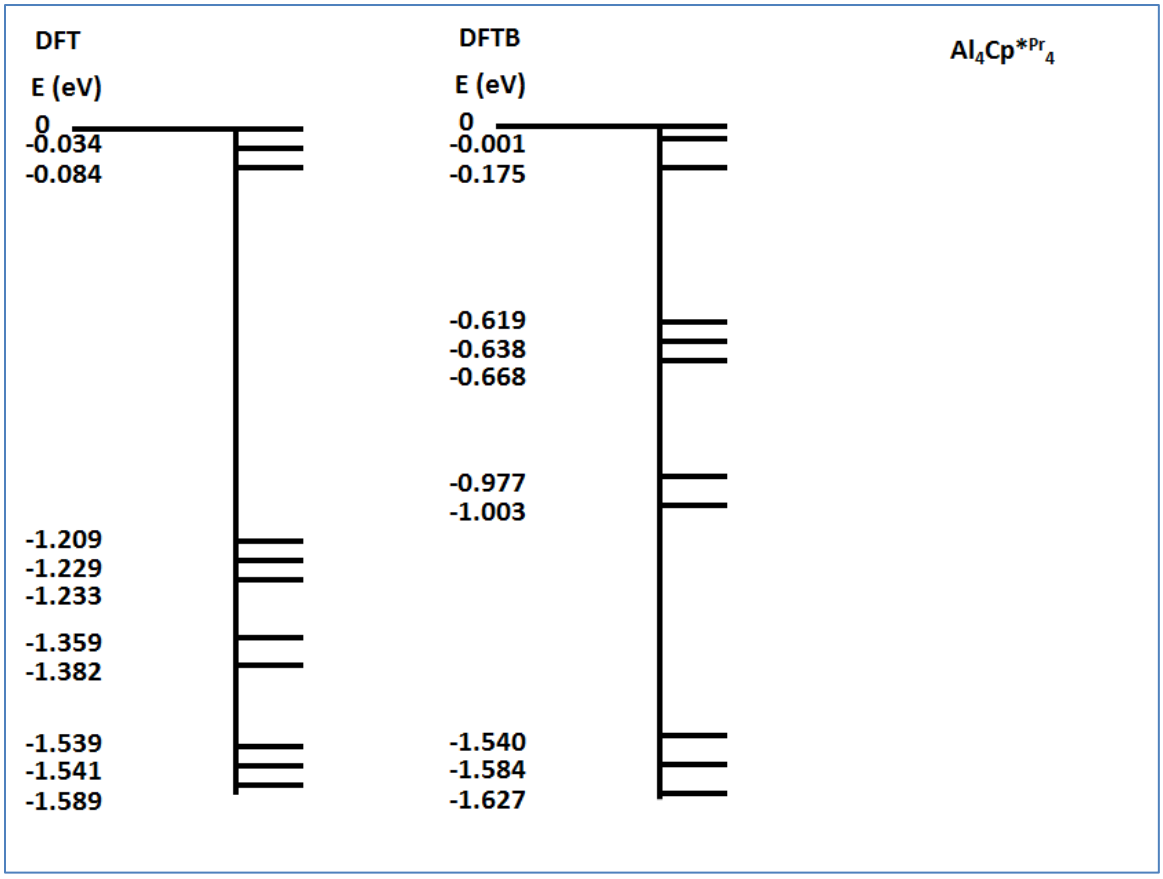

Figure 22. $Al_4Cp^{*Pr}_4$ Energy Levels

A general trend is established for the energy levels of the tetramer family of systems as presented in Figure 20, Figure 21, and Figure 22. The first two energy levels below the HOMO are in relatively good agreement between DFT and DFTB. However, the subsequent 3 energy levels are significantly underestimated, with the difference from DFT and DFTB ranging from approximately 0.6 to 0.8 eV. The next two energy levels have a difference with a much wider range, with the underestimation from DFT to DFTB starting at approximately 0.4 eV for $Al_4Cp^{*Pr}_4$ and going to approximately 0.8 eV for Al_4Cp_4. The subsequent three energy levels are underestimated by approximately 0.4 eV for Al_4Cp_4 going from DFT to DFTB, and is in generally good agreement between the two methods for $Al_4Cp^*_4$ and $Al_4Cp^{*Pr}_4$.

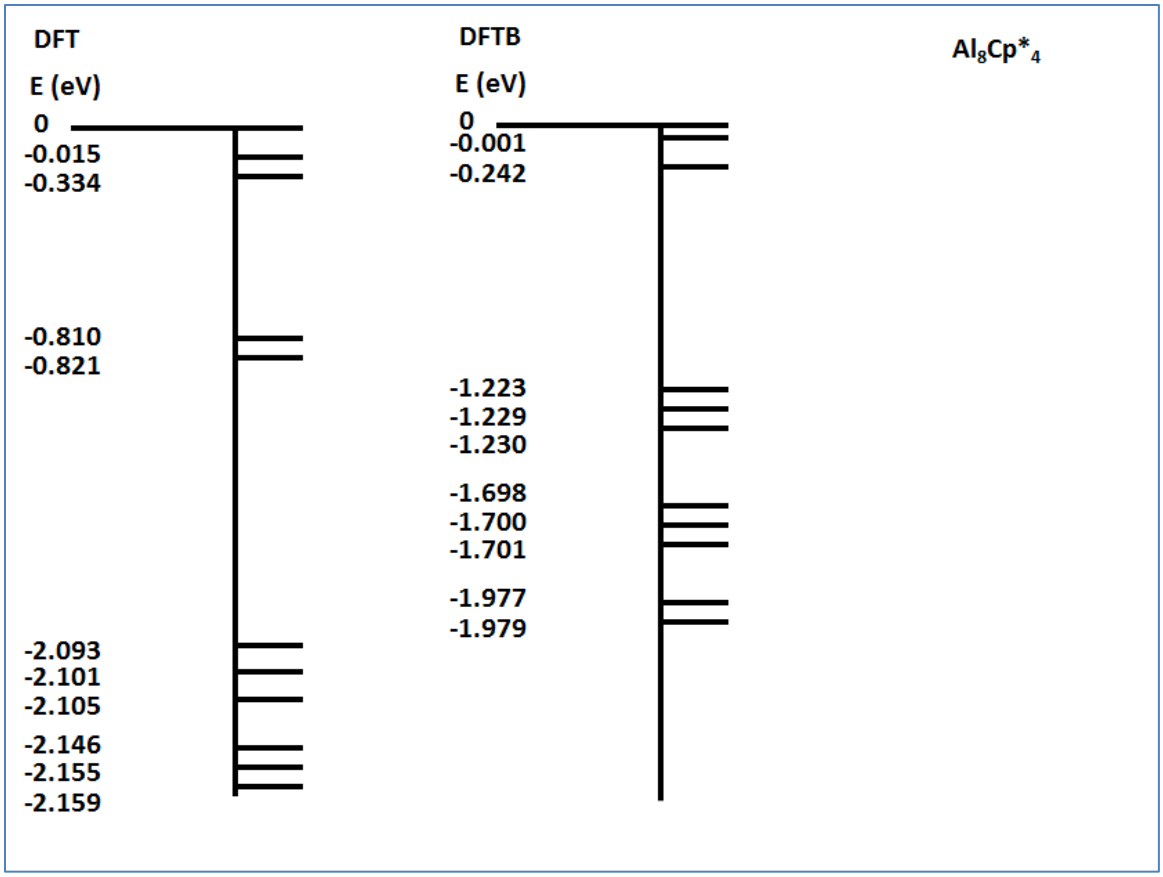

Figure 23. $Al_8Cp^*_4$ Energy Levels

The $Al_8Cp^*_4$ is the first indication of problems in matching the degeneracy of energy levels. As we see in Figure 23, after the first two energy levels below the HOMO, the groupings of energy levels breaks down. Overall, we see that the performance of the energy level calculations becomes more and more problematic as the complexity of our system increases, particularly as we introduce additional Al atoms to the system. As seen with the orbital plots, we believe that the minimal basis set requires us to conduct a re-parametrization of some key interactions to improve our performance for more complex systems.

D. MOLECULAR DYNAMICS

Recently our group has performed large-scale ab initio molecular dynamics of the oxidation of $Al_4Cp^*_4$ using a DFT-based Car-Parrinello method. This simulation, which

several months on the DOD supercomputers, was able to successfully predict many of the major decomposition products of this cluster and was validated by recent experimental studies. In this section we discuss efforts to use this newly developed potential to more efficiently simulate chemistry in Al/Cp clusters. We performed molecular dynamics in DFTB+ with a canonical (NVT) ensemble for the Al_4Cp_4 system and an $Al_3O_2Cp^*_3$ system, which is the initial expected reaction product of the Al_4Cp_4 cluster with an O_2 molecule. An Andersen thermostat was used, and the system was advanced using a velocity Verlet algorithm with a timestep of 0.05 femtoseconds.

The purpose of the Al_4Cp_4 simulation was to observe an equilibration of the system at a temperature of 300K, and determine if the system is stable against distortions when "annealed" with a simulated temperature. In Figure 24a below, we see the initial state of the system. From this starting configuration, we see that at 5 ps, in Figure 24b, one of the ligands has exhibited significant movement from its starting position in the tetramer. By the termination of the run at 25 ps, we see that another ligand, near the bottom left of the view in Figure 24c, demonstrates movement from its starting position as well. This suggests that the improved structures with the new potential may be in a local minimum, and that if given sufficient thermal energy we may again find distortion away from the known Al-Cp bond configuration. In future work a simulated annealing run using constant temperature MD is recommended as an improved check on the repulsive potential fits.

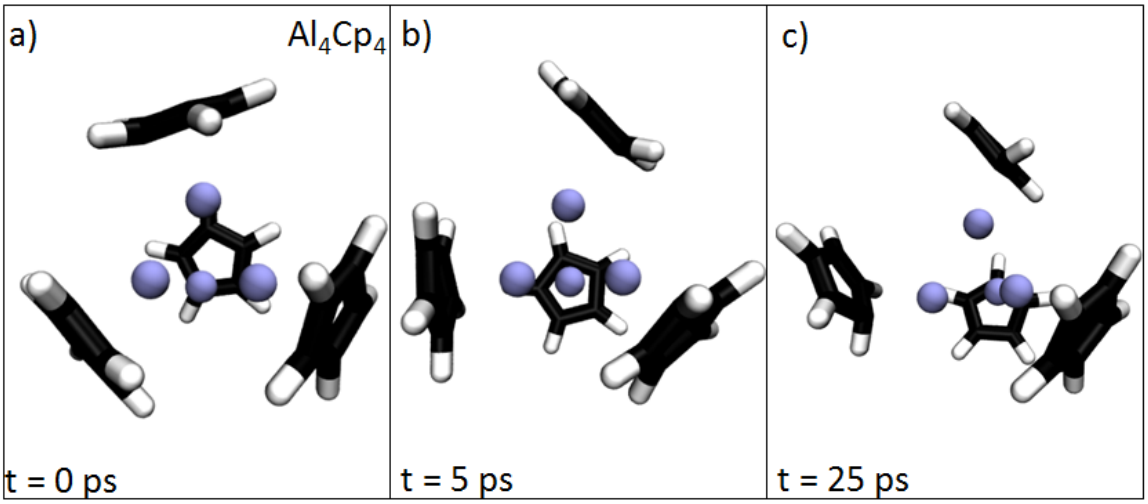

Box a) depicts the initial state of the system, Box b) depicts the system at 5 ps into the run, and Box c) depicts the system at the termination of the run at 25ps. Note the shifting in the top ligand position from Box a) to b), and then the shifting of the bottom left ligand position from Box b) to c).

Figure 24. Al_4Cp_4 Molecular Dynamics

We also simulated the molecular dynamics of the $Al_3O_2Cp^*_3$ reacted product. In Figure 25a we can see the starting configuration of the system. Figure 25b depicts the system after 5ps of simulation time, and we see that the ligands have begun to shift slightly. In Figure 25c, after 10.7ps, we see an encouraging result in which a hydride transfer from one of the Cp^* methyl groups to an Al center. This reaction also occurs in the DFT simulations, and there is indirect evidence for it in recent hot-write T-jump/mass spec experiments performed at University of Maryland on small quantities of the tetramer. In Figure 25d, after 15ps, we can see a second hydride has broken off to bond with another Al atom. In Figure 25e, a third hydride transfer has occurred. In Figure 25f, the ligands appear to have detached from the core, and the core has straightened into a new geometry. Though these results do not exactly reflect the DFT results, this DFTB simulation provides a very reasonable approximation of the reaction geometry seen in DFT, and captures some of the difficult effects such as the hydride transfer.

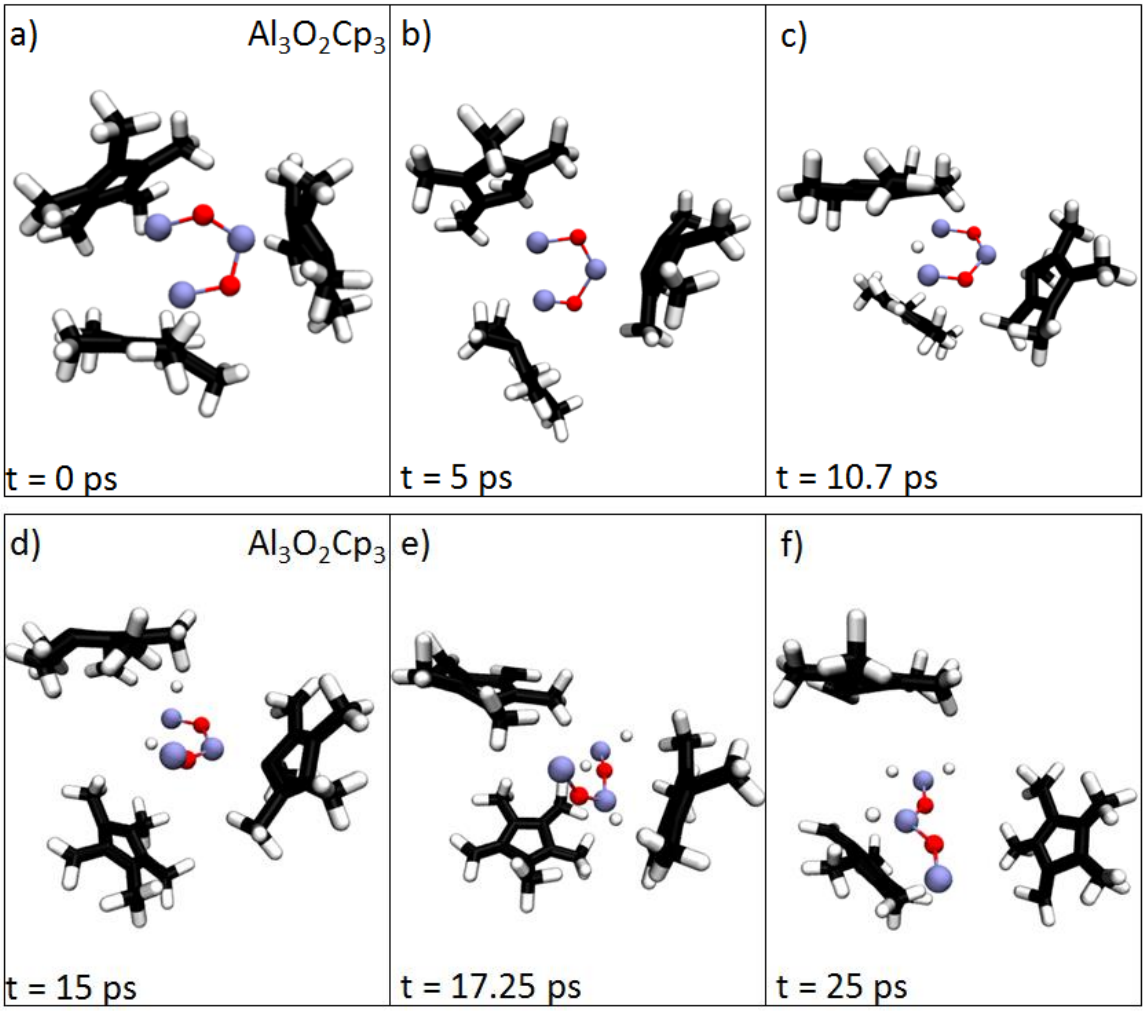

Box a) depicts the initial state of the system, Box b) depicts the system at 5 ps into the run, Box c) depicts the system at 10.7 ps, Box d) depicts the system at 15ps, Box e) depicts the system at 17.25 ps, and Box f) depicts the system at the termination of the run at 25ps. Note the H atom transfer in Box c), another H atom transfer in Box d), and a third H atom transfer in Box e). Box f) depicts the final configuration, where the ligands appear to have detached from the core, which has reconfigured into a new geometry.

Figure 25. $Al_3O_2Cp_3$ Molecular Dynamics

THIS PAGE INTENTIONALLY LEFT BLANK

V. CONCLUSIONS

A. PERFORMANCE

We have demonstrated that it is possible to significantly improve the performance of DFTB for the aluminum cyclopentadienyl family of clusters with the re-parametrization of just a single element pair interaction. Though our new parametrization demonstrates some shortfalls in more complex systems, we were looking to gain the most return on effort by targeting the most egregious shortcomings, and that this is far from a full and thorough re-parametrization.

The geometry optimization was the most significant improvement provided by the Al-C re-parametrization. In particular, we were able to correct the gross geometry distortions produced by the stock matsci-0-3 parameter set in the monomers. With a testing process to fine tune the re-parametrization, we were able to extend this improvement to more complex geometries, such as the tetramers. While we saw a loss in accuracy as we moved to even more complex geometries, the distortions did not appear to progressively grow worse as the system complexity grew and the optimized geometries were still reasonably accurate.

Molecular orbitals results were less ideal. Though we saw good accuracy in the orbitals for monomers, increasing complexity to tetramers led to grossly inaccurate distortions. In addition, energy levels were not in good agreement with DFT results. Molecular dynamics showed considerable promise for future research. Though not in perfect agreement with DFT, the reaction process for the reacted product simulated with reparametrized DFTB captures some of the key features seen in a DFT result.

B. FUTURE WORK

The tremendous reduction in the computational requirement provided by DFTB for these systems is a powerful incentive for further refinement of this method. The geometry optimization of the $Al_{50}Cp^*_{12}$ system was performed in under 24 hours with DFTB on a single processor, a process that can take thousands of CPU hours with higher level levels of DFT. Similar gains in processing time were seen in the molecular

dynamics simulations, with each run taking under 72 hours, in contrast to DFT run times measured in months.

For future work, it is recommended that a more thorough re-parametrization be conducted based on performance metrics beyond geometry optimization. There are several other parameters that can be adjusted in a subsequent attempt to improve performance. To improve the geometry results, additional improvements to accuracy could be gained by reparametrizing other interactions in the systems. Additionally, refinements to the band structure energy or Coulomb energy through adjusting the DFT method used or parameters such as the Hubbard parameter or electronegativity could improve the electronic structure calculations and reduce the magnitude of "correction" characterized in the repulsive potential. Lastly, the Al-C interaction demonstrated that geometry results were highly sensitive to even small changes in the parametrization. Therefore, a spline fit may offer better results by allowing adjustments to more easily focus upon the interaction region of interest.

APPENDIX A. FUNDAMENTAL CONSTANTS

$1\ \text{Ha} = 27.2114\ \text{eV}$

$1\ \text{Bohr} = 0.5292\ \text{Å}$

$1\ \text{u} = 1.6605 \times 10^{-27}\ \text{kg}$

Time: 1.0327 fs

With Hartree atomic units, the following constants are unity by definition:

m_e (electron mass)

e (elementary charge)

ħ (reduced Planck's constant)

k_e (Coulomb's constant)

THIS PAGE INTENTIONALLY LEFT BLANK

APPENDIX B. ALUMINUM-CARBON REPARAMETRIZATION

0.00, 0.0352 -0.067 0.0585 -0.0273 0.0069 -0.0010 0.0001 0, 6.81, 10*0.0

The above text is line 2 of the Al-C .skf file which contains the re-parametrization of the Al-C interactions. This line is manipulated identically in the similar C-Al .skf file. The formatting used for this interaction is the hetero-nuclear case in the DFTB skf documentation.

The first portion (0.00,) is a placeholder, and is used for atomic mass in homo-nuclear cases. The second portion (0.0352 -0.067 0.0585 -0.0273 0.0069 -0.0010 0.0001 0,) is the polynomial, with the input values reflecting the c_n coefficient values. The next portion (6.81,) is the cutoff radius, and these values are specified in Bohr. The final portion (10*0.0) is just a placeholder.

This line of the file would be modified to adjust the repulsive potential portion of the DFTB parametrization.

THIS PAGE INTENTIONALLY LEFT BLANK

LIST OF REFERENCES

[1] D. Mayo. (2015, Dec. 28). *Aluminum cluster materials are the future of energetics* [Online]. Available: http://futureforce.navylive.DODlive.mil/2015/12/aluminum-cluster-materials/

[2] J. Vollet, J. R. Hartig, and H. Schnöckel. "Al(50)C(120)H(180): a pseudofullerene shell of 60 carbon atoms and 60 methyl groups protecting a cluster core of 50 aluminum atoms," *Angew. Chem., Int. Ed.*, vol. 43, pp. 3186–3189, 2004.

[3] P. Koskinen and V. Mäkinen. "Density-functional tight-binding for beginners," *Computational Materials Science*., vol. 47, pp. 237–253, Jul. 2009.

[4] F. Shimojo, R. V. Kalia, A. Nakano, P. Vashista. "Linear-scaling density-functional-theory calculations of electronic structure based on real-space grids: design, analysis, and scalability test of parallel algorithms," *Computer Physics Communications*, vol. 140, pp. 303–314, Apr. 2001

[5] V. Mäkinen, P. Koskinen, H. Häkkinen. "Modeling thiolate-protected gold clusters with density-functional tight-binding," *The European Physical Journal D*, vol. 67, no. 38, Feb. 2013.

[6] B. Aradi, B. Hourahine, and T. Frauenheim. "DFTB+, a sparse matrix-based implementation of the DFTB method," *The Journal of Physical Chemistry A*, vol. 111, pp. 5678–5684, Jan. 2007.

[7] J. Frenzel et al. "Semi-relativistic, self-consistent charge Slater-Koster tables for density-functional based tight-binding (DFTB) for materials science simulations." Technical University-Dresden 2004–2009. Available: http://www.dftb.org/parameters/download/matsci/matsci-0-3/

[8] R. Luschtinetz et al. "Adsorption of phosphonic and ethylphosphonic acid on aluminum oxide surfaces," *Surface Science*, vol. 602, pp. 1347–1359, 2008.

[9] *Format of the v1.0 Slater-Koster files*. DFTB+. [Online]. Available:http://www.dftb.org/fileadmin/DFTB/public/misc/slakoformat.pdf

[10] J. S. Nokelainen. "Computational modelling of boron nitride nanostructures based on density-functional tight-binding," M.S. thesis, Dept. Physics, University of Jyväskylä, Jyväskylä, Finland, 2014.

[11] P. H. M. Budzelaar, J. J. Engelberts, and J. H. van Lethe. "Trends in cyclopentadienyl-main group metal bonding." *Organometallics*, vol. 22, pp. 1562–1576, Nov. 2003.

[12] J. P. Perdew and M. Levy. “Physical content of the exact Kohn-Sham orbital energies: band gaps and derivative discontinuities,” *Physical Review Letters*, vol. 51, no. 20, Nov. 1983.

[13] K. S. Williams and J. P. Hooper. “Structure, thermodynamics, and energy content of aluminum-cyclopentadienyl clusters.” *The Journal of Physical Chemistry A*, vol. 115, pp. 14100-1419, Oct. 2011.

[14] D. Mayo and B. Eichhorn, private communication, May 2016.

INITIAL DISTRIBUTION LIST

1. Defense Technical Information Center
   Ft. Belvoir, Virginia

2. Dudley Knox Library
   Naval Postgraduate School
   Monterey, California